Deep carbon through time: Earth's diamond record and its implications for carbon cycling and fluid speciation in the mantle

D. Howell[1,2,3], T. Stachel[1], R.A. Stern[1], D.G. Pearson[1], F. Nestola[2], M.F. Hardman[1], J.W. Harris[4], A.L. Jaques[5], S.B. Shirey[6], P. Cartigny[7], K.V. Smit[8], S. Aulbach[9], F.E. Brenker[9], D.E. Jacob[10], E. Thomassot[11], M.J. Walter[12], O. Navon[13]

1 Department of Earth and Atmospheric Sciences, University of Alberta, Edmonton, Alberta T6G 2E3, Canada
2 Department of Geosciences, University of Padova, Via Gradenigo 6, I-35131 Padova, Italy
3 Vrije Universiteit, De Boelelaan 1085, 1081 HV Amsterdam, The Netherlands
4 School of Geographical and Earth Sciences, University of Glasgow, Glasgow G12 8QQ, UK
5 Research School of Earth Sciences, Australian National University, 142 Mills Road, Acton, ACT 2601, Australia
6 DTM, Carnegie Institution for Science, Washington, DC20015, USA
7 Laboratoire de Geochimie des Isotopes Stables, Institut de Physique du Globe de Paris, Universite Paris Diderot, Centre National de la Recherche Scientifique, UMR 7154, Sorbonne Paris-Cite, 75238 Paris
8 Gemological Institute of America, 50 West 47th Street, New York City, NY 10036, USA
9 Institut für Geowissenschaften, Goethe-Universität, Frankfurt am Main, Germany
10 Australian Research Council Centre of Excellence for Core to Crust Fluid Systems and Department of Earth and Planetary Sciences, Macquarie University, North Ryde, New South Wales 2109, Australia
11 Centre de Recherches Petrographiques et Geochimiques, Centre National de la Recherche Scientifique, Universite de Lorraine, 54501 Vandœuvre-les-Nancy, France
12 Geophysical Laboratory, Carnegie Institution for Science, Washington, DC20015
13 Institute of Earth Sciences, The Hebrew University, Jerusalem 9190401, Israel

Abstract

Diamonds are unrivalled in their ability to record the mantle carbon cycle and mantle fO_2 over a vast portion of Earth's history. Diamonds' inertness and antiquity means their carbon isotopic characteristics directly reflect their growth environment within the mantle as far back as ~3.5 Ga. This paper reports the results of a thorough secondary ion mass spectrometry (SIMS) carbon isotope and nitrogen concentration study, carried out on fragments of 144 diamond samples from various locations, from ~3.5 to 1.4 Ga for P [peridotitic]-type diamonds and 3.0 to 1.0 Ga for E [eclogitic]-type diamonds. The majority of the studied samples were from diamonds used to establish formation ages and thus provide a direct connection between the carbon isotope values, nitrogen contents and the formation ages. In total, 908 carbon isotope and nitrogen concentration measurements were obtained. The total $\delta^{13}C$ data range from -17.1 to -1.9 ‰ (P = -8.4 to -1.9 ‰; E = -17.1 to -2.1 ‰) and N contents range from 0 to 3073 at. ppm (P = 0 to 3073 at. ppm; E = 1 to 2661 at. ppm). In general, there is no systematic variation with time in the mantle carbon isotope record since >3 Ga. The mode in $\delta^{13}C$ of peridotitic diamonds has been at -5 (± 2) ‰ since the earliest diamond growth ~3.5 Ga, and this mode is also observed in the eclogitic diamond record since ~3 Ga. The skewness of eclogitic diamonds' $\delta^{13}C$ distributions to more

negative values, which the data establishes began around 3 Ga, is also consistent through time, with no global trends apparent.

No isotopic and concentration trends were recorded within individual samples, indicating that, firstly, closed system fractionation trends are rare. This implies that diamonds typically grow in systems with high excess of carbon in the fluid (i.e. relative to the mass of the growing diamond). Any minerals included into diamond during the growth process are more likely to be isotopically reset at the time of diamond formation, meaning inclusion ages would be representative of the diamond growth event irrespective of whether they are syngenetic or protogenetic. Secondly, the lack of significant variation seen in the peridotitic diamonds studied is in keeping with modeling of Rayleigh isotopic fractionation in multicomponent systems (RIFMS) during isochemical diamond precipitation in harzburgitic mantle. The RIFMS model not only showed that in water-maximum fluids at constant depths along a geotherm, fractionation can only account for variations of <1 ‰, but also that the principal $\delta^{13}C$ mode of -5 ± 1 ‰ in the global harzburgitic diamond record occurs if the variation in fO_2 is only 0.4 log units. Due to the wide age distribution of P-type diamonds, this leads to the conclusion that the speciation and oxygen fugacity of diamond forming fluids has been relatively consistent. The deep mantle has therefore generated fluids with near constant carbon speciation for 3.5 Ga.

Keywords

Mantle carbon; isotope fractionation; mantle oxygen fugacity; diamond growth; deep carbon cycle; subduction.

Introduction

Carbon and other elements that form volatile species in Earth's mantle, such as nitrogen and hydrogen, are major constituents of our planet and, along with oxygen, dominate the composition of the atmosphere and hydrosphere. The cycling of these elements from the surface into the deep Earth via subduction, and then back to the surface via volcanism has been integral to regulating climate, ocean volume and the habitability of our planet. While many of these volatile cycles in the atmosphere, biosphere and crust are understood, the deeper aspects of these cycles in the mantle

and core are rather poorly constrained (Hazen & Schiffries, 2013). Of interest is the comparison between constancy of the surficial carbon isotope record (e.g. Des Marais, 2001) and that of the mantle through time because the mantle is - by more than an order of magnitude - a larger reservoir of C than the crust (e.g. Kelemen & Manning, 2015). By studying the fluxes between Earth's reservoirs we gain valuable insights into the geological processes of subduction, partial melting, degassing and metasomatism, and by tracing these processes back through time we gain further insight into the evolution of our planet.

The upper mantle's redox state is intimately linked to the evolution of Earth's atmosphere through volcanic degassing (Kasting et al., 1993). Potential variations in the mantle's oxidation state through time therefore have significant consequences, yet this has been a controversial topic for many decades (McCammon, 2005; Frost & McCammon, 2008; Foley, 2011). Most of the controversy lies in the fact that oxygen fugacity information obtained from the study of volcanic rocks does not agree with that obtained from the study of mantle peridotites (see Figure 1 of Foley (2011) and references therein). Determining mantle fO_2 from $Fe^{3+}/\sum Fe$ analyses on ancient peridotites and mid-ocean ridge basalts (MORB) is problematic due to the independent or combined effects of alteration and metasomatism. As a result, trace element systematics, such as V, Cr, Sc and Ce, have been employed to estimate oxygen fugacity (fO_2; Canil, 1997; Li and Lee, 2004; Trail et al., 2011). Many studies of upper mantle-derived rocks have concluded that mantle fO_2 has remained constant, within ~1 log unit of the fayalite-magnetite-quartz (FMQ) oxygen buffer at 1 GPa, since 3.5 Ga (Canil, 1997; Canil and Fedortchouk, 2001; Delano, 2001; Li and Lee, 2004; Berry et al., 2008; Trail et al., 2011; Hibbert et al., 2012; Rollinson et al., 2017; Nicklas et al., 2018). However, the comprehensive review by Foley (2011) along with some recent studies (Aulbach & Viljoen, 2015; Aulbach & Stagno, 2016; Shu et al., 2016; Aulbach et al., 2017; Nicklas et al. 2019) have suggested that the Archean mantle was more reducing than that of the present day. These contrasting results highlight the uncertainty in our knowledge of fO_2 through time.

Along with potential temporal variation in the mantle's oxygen fugacity, there are also vertical variations to consider. The effects of pressure cause the mantle to become more reducing with depth (Ballhaus & Frost, 1994). The implications of this

variation for carbon are that at more oxidised (higher fO_2) conditions in the shallow mantle, carbonate and CO_2 would be the stable / dominant species, changing to CH_4 and metallic carbide with decreasing fO_2 (and depth). Therefore variation of mantle fO_2 through time has implications for the speciation of carbon-related volatiles in the upper mantle.

Diamonds are unrivalled in their ability to record the mantle carbon cycle over a vast portion of Earth's history. They are the product of ascending, cooling, carbon-saturated metasomatic fluids-melts and/or redox reactions, predominantly within peridotitic and eclogitic domains in the mantle lithosphere (see Stachel & Luth (2015) and references therein). Their occurrence with inclusions of CO_2 (Schrauder & Navon, 1993), carbonate (e.g. Wang et al., 1996), methane (Smit et al., 2016) and carbide (e.g. Mikhail et al., 2014; Smith et al., 2016), show their formation over a significant range of oxygen fugacities. However, the lack of buffering capacity of peridotitic subcratonic mantle (Luth & Stachel, 2014) suggests that redox reactions may not be responsible for diamond growth in this part of the mantle. Luth & Stachel (2014) showed that the speciation of carbon in mantle fluids is actually the controlling variable when it comes to the oxygen fugacity of the peridotitic lithospheric mantle, which is counter to the traditional view of the fluids adjusting to the prevalent fO_2 rather than buffering them (e.g. Woodland et al. 2006). Understanding the role of carbon-bearing melts in eclogitic domains and their relationship to fO_2 is inherently more complex and the subject of ongoing study.

A key characteristic that makes diamond such a powerful tool for studying the mantle is that once grown, they do not chemically re-equilibrate with their surroundings. This means their carbon isotopic composition, as well as their potential load of nitrogen, hydrogen, boron and nickel impurities, directly reflect their growth environment. Given that diamond growth events have been dated as far back as ~3.5 Ga (Figure 1: see Supplementary Material Table S1 and references therein), no other mineral can provide such detailed insight into mantle fluid processes and the deep carbon cycle throughout Earth's evolution.

The historical database of diamond carbon isotope compositions (e.g., Cartigny et al., 2014) is based on the bulk analysis of diamond fragments. Bulk C-isotopic analyses,

combined with FTIR nitrogen analyses, have been successfully employed in some instances to track Rayleigh fractionation processes during diamond formation (Cartigny et al., 2001; Thomassot et al., 2007; Stachel et al., 2009). The homogeneity of carbon isotope values (± 2 ‰) in the majority of diamonds studied has been shown by comparing data from multiple fragments of the same samples (see figure 5 of Cartigny et al., 2004). Stepped combustion analysis of individual samples also revealed limited heterogeneity in carbon isotopes values (Mikhail et al., 2014) but lacked spatial resolution. The development of secondary ion mass spectrometry (SIMS) methods applicable to measuring carbon isotopes of diamonds *in situ* from very small analytical volumes (Harte & Otter, 1992; Fitzsimmons et al., 1999; Hauri et al., 2002), showed clearly that a few gem diamonds had very heterogeneous carbon isotopic values depending on their growth history (Harte et al., 1999; Bulanova et al., 2002; Zedgenizov & Harte, 2004). Considering the observed diamond internal heterogeneity on the micron scale (e.g. Fitzsimmons et al., 1999), the most accurate approach to determine the possible fluid speciation in diamond-forming fluids is to measure spatially resolved growth-directional trends (i.e. core to rim) in the carbon isotopic and nitrogen concentration systematics in individual diamonds (e.g. Smart et al., 2011; Wiggers de Vries et al., 2013; Smit et al., 2016; 2019a).

This paper reports the results of a major SIMS carbon isotope study, carried out on 144 diamond samples, spanning a large range of geological time (~3.5 to 1.4 Ga for P-type diamonds, 3.0 to 1.0 Ga for E-type diamonds). The sample collection studied provides a direct connection between the ages of diamond formation, obtained from inclusion studies, and the carbon isotope values of the host diamonds. The spatial resolution of the analyses, together with the readily identifiable core to rim growth directions evident in most samples, allows trends in the variability of C isotopic values and nitrogen concentrations to be examined, with the goal to search for possible systematic shifts in the speciation of carbon-bearing mantle fluids through time.

Samples

Fragments of 144 diamond crystals, from nine localities in Canada, Australia, Southern Africa and Russia, have been analysed for their carbon isotopic values and nitrogen contents. Of those, 88 are defined as having a peridotitic association (P-type) based upon their inclusion paragenesis, and 56 formed in eclogitic substrates (E-type). The details of the sample source locations are provided in Table 1, along with references to the original studies that dated the inclusions. With the exception of 18 samples from Diavik (Slave Craton, Canada; Donnelly et al., 2007), 11 from Wawa (Superior Craton, Canada; Stachel et al., 2006), 13 from Ellendale (Kimberley Craton, Australia; Jaques et al., 1989; 1994), and 10 from Argyle (Kimberley Craton, Australia; Stachel et al., 2018), the remaining majority of the diamonds studied here are fragments, recovered after breakage to obtain inclusions for dating studies. Therefore, they can be directly linked to the age of the diamond growth event documented in the original dating study.

For peridotitic diamonds from De Beers Pool, Udachnaya and Venetia, diamond formation ages come from radiogenic isotope analysis of pooled garnet inclusions (Richardson et al., 1984; Richardson & Harris, 1997; Richardson et al., 2009). For eclogitic diamonds from De Beers Pool (Bultfontein, De Beers, Dutoitspan, and Wesselton kimberlites), Jwaneng and Orapa, ages were obtained by Re-Os analysis of individual sulphide inclusions (Richardson et al., 2001; 2004; Shirey et al., 2009). In the case of the Diavik, Argyle and Ellendale diamonds, which are not directly derived from age dating studies on these diamond populations (Aulbach et al., 2009; Richardson, 1986; Smit et al., 2010), the inclusion compositions and N aggregation characteristics are similar to the original suites used for geochronology and thus the published ages are applied. The diamonds from Wawa have not been dated directly but are constrained by the age of the rocks they are found in (~2.7 Ga; Stachel et al., 2006) as being Neoarchean, which obviously represents a minimum age. All of the diamonds (with the possible exception of two Wawa diamonds with majoritic garnets) are lithospheric (140 – 250 km) in origin.

Whilst Thomassot et al (2009) argue that at Jwaneng silicate- and sulphide-bearing diamonds form in separate events, the presence of silicate and sulphide inclusions (in part even touching; Richardson et al., 2004) in the same P and E-type diamonds at Jwaneng strongly suggests coeval formation. Even if silicate- and sulphide-bearing

diamonds formed during different growth events, this would have very limited implications for this study because all of the peridotitic diamond samples that are directly tied to the dating studies contained only silicate inclusions, while all directly dated eclogitic samples are sulphide-bearing. For the three P-type sample collections with indirect ages (Diavik, Ellendale and Wawa), only 4 of the diamonds contained sulphides (1 from Diavik, 3 from Ellendale). For the E-type sample collections with indirect ages (Diavik and Argyle), all 10 Argyle samples are silicate-bearing (in keeping with the dating study which used silicates) and 4 of the 9 Diavik samples are silicate-bearing (not in keeping with the sulphide derived age). So with the exception of 8 samples, the remainder are all in keeping with the inclusion type used to obtain the age. The peridotitic samples represent silicate-bearing diamond formation events, while excluding Argyle, the remaining eclogitic samples represent sulphide-bearing diamond formation events.

Given that all of the diamonds studied here are fragments, they do not record the crystals' entire growth history. During selection and mounting, every effort was made to discern an outer crystal surface, so that the subsequent analysis would have a context of growth direction and data transects would represent the evolution of the crystal's growth. Data from 96 samples have confirmed growth direction context, supported by cathodoluminescence (CL) imaging of their growth structure.

Fibrous and polycrystalline diamonds are assumed to form during unusually rapid crystal growth driven by strong supersaturation in carbon. Fibrous diamonds are most likely of young (Phanerozoic) geological age (Sunagawa, 1984; Gurney et al., 2010), while no polycrystalline diamonds have ever been dated. Such young and undated diamond types cannot be used to constrain variations in the carbon isotopic composition of diamonds through time, and they are therefore not included in the present study, nor are the literature data derived from those types of samples. Similarly, microdiamonds (generally defined as <0.5 mm) are also not included as age data are not available.

Methods

Mount preparation, CL imaging and secondary ion mass spectrometry (SIMS) were carried out at the Canadian Centre for Isotopic Microanalysis (CCIM), University of Alberta. Four SIMS mounts were created and analyzed in this study (M1369, M1406, M1410, M1520). The rough diamond fragments were cast together in groups of 20 to 50 in 25 mm epoxy discs, and ground and polished using electroplated diamond pads on rotary equipment to expose flat sections through grain interiors. These epoxy discs containing polished diamonds were trimmed to mm-scale blocks and pressed into SIMS indium mounts (M1369, M1410, M1520) along with a piece of CCIM diamond reference material (RM) S0270 and vitreous carbon S0233A. For epoxy mount M1406, reference materials were pressed into an integrated indium slot within an epoxy mount. In all cases, the RMs and unknowns were spaced closely together on each mount. The SIMS mounts were coated with ~20 nm of Au prior to scanning electron microscopy (SEM) using a Zeiss EVO MA15 instrument, operating at 15 kV and ~3 nA beam current. CL SEM images were obtained using a parabolic mirror coupled to a high-sensitivity, broadband photomultiplier detector. The mounts were subsequently coated with additional Au prior to SIMS analysis.

Isotopes of carbon ($^{13}C/^{12}C$) were determined using the IMS-1280 multi-collector ion microprobe at CCIM. Analytical methods and reference materials are detailed in Stern et al. (2014). Primary beam conditions included the use of 20 keV $^{133}Cs^{+}$ ions focused to a diameter ~ 15 µm and beam currents of ~ 2.0 nA. The primary beam was rastered across a 20 x 20µm area for 30 s prior to analysis, to clean the surface of Au and contaminants, and implant Cs. The normal incidence electron gun was not utilized, as most diamonds are conducting under ion bombardment. Negative secondary ions were extracted through 10 kV to the grounded secondary column (Transfer section). Automated tuning of the secondary ions in the Transfer section preceded each analysis. Secondary ion collection conditions for C-isotopes included an entrance slit width of 100 µm, field aperture of 5 x 5 mm, a field aperture-to-sample magnification of 100 x, and a fully-open energy slit. Both $^{12}C^{-}$ and $^{13}C^{-}$ were analyzed simultaneously in Faraday cups (L'2 and FCs using 10^{10} Ω and 10^{11} Ω amplifier circuits) at mass resolutions of 2000 and 2900, respectively. Faraday cup baselines were determined once at the start of the session. Mean count rates for $^{12}C^{-}$ and $^{13}C^{-}$ were typically 1.1–1.6 x 10^{9} and 1.2–1.8 x 10^{7} counts/s, respectively, determined over a 75 s counting interval, with total analysis time of 210 s. The analytical sequence

interspersed measurements of unknowns with the natural diamond S0270, having $\delta^{13}C_{VPDB}$ = -8.88 ±0.10 ‰ in a 4:1 ratio. Instrumental mass fractionation (IMF) for $^{13}C^-/^{12}C^-$ is typically about -24 ‰, determined precisely for each session from utilizing all the replicate analyses of S0270 diamond time-corrected back to the start of the sub-session. The standard deviation of the $^{13}C^-/^{12}C^-$ values per session was ±0.05 – 0.07 ‰ after correction for systematic within-session IMF drift of ≤0.5‰ over several hours. Uncertainties of individual $\delta^{13}C_{VPDB}$ analyses propagate within-spot (~±0.04‰, 1σ), between-spot (±0.05‰, 1σ), and between-session errors (±0.01‰, 1σ), and average ±0.14 ‰ (2σ).

Nitrogen abundances were determined for some diamonds immediately following C-isotope analysis from the identical spot locations. The primary beam was rastered for 30 –60 s prior to analysis to clean the adjacent area. Secondary ion collection conditions included an entrance slit width of 45 µm, field aperture of 3 x 3 mm, and energy slit width of 40 eV transmitting low-energy ions. The molecular ion ratios of $[^{12}C^{14}N^-]/[^{12}C^{12}C^-]$ or $[^{13}C^{14}N^-]/[^{12}C^{13}C^-]$ were analyzed simultaneously using either a Faraday cup–Faraday cup (L'2–FC2) or Faraday cup–electron multiplier combination (L'2–EM). Mass resolution was ~6300 – 7000 for CN^- molecular ions, 2100 for $^{12}C^{12}C^-$, and 6000 for $^{12}C^{13}C^-$. Electron multiplier counts were corrected for background and deadtime (40 ns). Total analysis time was 200 – 240 s, including pre-analysis raster, secondary ion centering, and peak counting time of 25 – 50 s. The sensitivity factor for N in diamond was determined by analysis of S0280 diamond having nitrogen concentration ([N]) = 1670 at. ppm located on a separate mount (Stern et al., 2014), or analysis of S0270 diamond with ~2150 at. ppm located on the same mount. Uncertainties in concentration are ±5 % absolute (95% conf.)

Results

In total, 908 combined carbon isotope and nitrogen concentration measurements have been obtained for peridotitic (n = 504) and eclogitic (n = 404) inclusion-bearing diamonds. The entire dataset is provided in the Supplementary Material, grouped according to inclusion paragenesis (Table S2). Histograms of the $\delta^{13}C$ data (Figure 2) are given per location and age, while the statistical characteristics are provided in

318 Table 2. The $\delta^{13}C$ data range from -17.1 to -1.9 ‰ (P -8.4 to -1.9 ‰; E -17.1 to -2.1
319 ‰) and N contents range from 0.4 to 3073 at. ppm (P 0.4 to 3073 at. ppm; E 1 to 2661
320 at. ppm).
321
322 As a different number of analyses were recorded per sample, there is potential for a
323 sample bias to become incorporated in the population data through overrepresentation
324 of one sample's characteristics relative to another sample. For example, in the
325 literature the presence of highly negative (<-15 ‰) portions within a diamond are
326 commonly studied by SIMS in much greater detail than the often more dominant
327 mantle like (~-5 ‰) volumes as they are of greater potential interest in defining the
328 source of the carbon, resulting in a strongly bimodal distribution in some datasets,
329 which is proportionally misleading. To check for this within this study, the average of
330 each sample's C and N characteristics were calculated as well as their median values,
331 and then averaged to compare against the whole population per location. It is clear
332 from the values shown in Table 2 that overrepresentation is not a significant issue for
333 the $\delta^{13}C$ and N concentration data reported here.
334
335 From the CL images it is possible to tell that the vast majority of diamonds with
336 sufficient nitrogen content to luminesce are dominated by octahedral growth. Some
337 samples from Diavik (n = 3), Venetia (n = 1), De Beers Pool (n = 1), Jwaneng (n = 4)
338 and Orapa (n = 1) also reveal some portions of cuboid growth, identified by having a
339 CL response consistent with previous studies of cuboid growth (e.g. Welbourn et al.,
340 1989; Howell et al., 2012). However, as there is no evidence of carbon isotopic
341 fractionation between cuboid and octahedral sectors in mixed-habit diamonds (Howell
342 et al., 2013) this observation does not affect the present data. [N.B. No fibrous
343 diamond material was analysed within this study.] The CL images also reveal that the
344 sample collection is quite varied in terms of the growth history of individual
345 diamonds (Figure 3). Nearly half of the diamonds studied here (71 of 144) clearly
346 exhibit either pulsed growth (repetitive subtle variations in CL response; not clear if
347 single or multiple growth events) or clear discrete multiple growth events (noted by a
348 marked difference in CL response as well as resorption features). Complex histories
349 involving multiple growth stages are not necessarily accounted for in the defined ages
350 of the samples, given the rarity of multiple inclusion-bearing diamonds with
351 inclusions in more than one growth zone and that many of the P-type diamond

formation ages were determined from pooled silicate inclusions from many diamonds, as opposed to techniques of dating individual sulphide or silicate inclusions (e.g. Pearson et al., 1998; Timmerman et al., 2017).

Four of the samples exhibiting multiple growth events (all E-type; ddmi-37, JWR7, JWR13, JWR22) show a jump in the $\delta^{13}C$ values between two layers of >3 ‰; the lowest isotopic values are found in the core of the stone, with subsequent overgrowth having less negative $\delta^{13}C$ values. If the $\delta^{13}C$ data for these four samples are removed from the dataset presented in Table 2, then the average Δ values (where Δ represents the variation within individual samples) for E-type diamonds from Diavik (1.9 Ga) and Jwaneng (3 Ga and 2.1 Ga) change to 0.4 ‰ (from 1.0 ‰), 1.5 ‰ (from 3.7 ‰) and 1.4 ‰ (from 2.5 ‰), respectively. This reduces the average Δ value of the E-type population to 1.2 ‰ from 1.6 ‰ (calculated from the average Δ values of the nine diamond growth events from the five localities, as opposed to the average Δ values of all 52 individual samples). Given that the average Δ value of the P-type population is 0.8 ‰, this implies that intra-sample variation is typically slightly higher in E-type diamonds than in the P-type diamonds studied here.

To investigate whether the presence of multiple growth events in half of the diamonds affects the dataset as a whole, the data from samples revealing only a single growth event (Table 3) were plotted as histograms (for the P-type and E-type populations) and compared against the total dataset (Figure 4). The single-phase growth peridotitic data (52 samples out of the 88) show a very similar distribution to the total P-type data set. The mean (-4.7 ‰) and median (-4.8 ‰) values of the single growth data are only slightly higher for than the total dataset (-4.8 ‰ and -4.9 ‰, respectively), with their standard deviations being very similar; 1.1 (total dataset) to 1.2 (single growth). For the E-type single-phase growth data (21 samples out of 56), the second mode in the $\delta^{13}C$ distribution at -12 to -9 ‰ is much more prominent than in the total dataset. The main reason for this is that the second mode around -10 ‰ is predominantly governed by the Argyle samples, which show less evidence for multiple growth events (4 out of 10 samples), while the Orapa (11 out of 13 samples) and Jwaneng (11 out of 16 samples) data, which are centred around -5 ‰, are greatly reduced (only 51 out of 233 analyses remain). Despite this more prominent bimodality in the single

385 growth data set, the mean of the single growth data is slightly higher (-6.6 ‰) than for
386 the total dataset (-6.7 ‰) whilst the median is slightly lower (-5.9 ‰ versus -5.7 ‰).
387 From this comparison, we conclude that the P-type dataset may be interpreted within
388 a temporal context without significant concern that the carbon signal could be biased
389 by multiple growth events being mis-classified into single time intervals. For the E-
390 type samples, the coupling of the published age data to the new carbon data is clearly
391 less robust due to a prevalence of multi-stage growth; this will need to be kept in mind
392 when interpreting the dataset as a whole, although the differences between the mean
393 and median of the single growth subset compared with the total dataset are small.
394
395
396 *Literature Data*
397
398 In the discussion section below, the P and E-type data from this study are compared
399 with that from the literature. Literature data predominantly represent "bulk" (typically
400 fragments of ≤1 mg) combustion analyses. We compiled a database containing ~2600
401 monocrystalline samples (i.e. excluding fibrous, polycrystalline and micro-diamonds),
402 which subsequently is referred to as the "*total literature data*".
403
404 Figure 1 shows that in addition to the present work there are more than 20 diamond
405 growth events (excluding fibrous growth) for which there is a geological age. To
406 expand both the number of growth events discussed and to compare the data
407 presented here with published data on the same deposits, we utilized data from the
408 literature. The key criterion for using literature data was that the mineral inclusion
409 paragenesis could be defined and clearly tied to a specific dated growth event. For
410 example, Finsch has an age for P-type diamond growth at 3.3 - 3.5 Ga (Richardson et
411 al., 1984) and for E-type growth at 1.5 Ga (Richardson et al., 1990), so carbon isotope
412 data for diamonds from this mine of known paragenesis (e.g. Appleyard et al., 2004;
413 Palot et al, 2013) can be attributed to either age. Conversely, Premier / Cullinan has
414 multiple growth ages for peridotitic paragenesis diamonds (see Figure 1) and since the
415 carbon isotope data cannot be tied to specific growth events, data from Cullinan
416 diamonds are not considered here.
417

A few studies with age constraints have utilized SIMS analysis, with multiple points per sample, namely the Zimmi (Sierra Leone) data from Smit et al. (2019a), the Koffiefontein data (Timmerman et al., 2019a) and some of the Finsch data (Palot et al., 2013), the latter two both from South Africa. In these cases, the number of samples is only 5, 3 and 10, but the number of individual analyses equate to 179, 12 and 113, respectively. The numbers of analyses and data statistics for the literature data discussed below are provided in Table 4, while all of the original data are compiled in the Supplementary Material (Table S3). This subset of literature data (combining 'bulk' and SIMS data from age constrained deposits) will be referred to as the "*dated literature data*".

Discussion

Carbon isotope systematics

The range of carbon isotope values recorded in the global bulk diamond database (i.e. total literature data) extends from -41 ‰ to +5 ‰ (see Cartigny et al., 2014 and references therein). The tight clustering of $\delta^{13}C$ data for peridotitic diamonds (95 % are within -5 ± 2.2 ‰) coincides with $\delta^{13}C$ data from other mantle sources (e.g. carbonatite and kimberlite carbonates, mid-oceanic ridge basalts, volcanic CO_2 emissions, mantle xenoliths; see Deines (2002) and references therein), leading to a general agreement that a $\delta^{13}C$ value of around -5 ‰ reflects the carbon isotopic signature of the upper mantle. The negative skewness of $\delta^{13}C$ data for eclogitic diamonds (~30 % are <-10 ‰) has been the source of debate for decades, and three different explanations have been proposed:

(1) Primordial heterogeneity within the mantle (Deines et al., 1993).

(2) The fractionation of carbon isotopes in an open system. This can occur either prior to diamond precipitation, where decarbonation may cause CO_2 enriched in ^{13}C to escape, leaving behind a ^{13}C-depleted fluid (Cartigny et al., 1998; 2001), or it may be a consequence of carbon isotope fractionation during diamond precipitation in a fluid-limited system (Deines, 1980).

(3) The recycling of crustal carbon via subduction, which has undergone fractionation by near-surface process to produce a very large range of carbon isotope values (Sobolev and Sobolev, 1980; Milledge et al., 1983; Kirkley et al., 1991).

The concept of primordial heterogeneity within the mantle was based on the observation that a single kimberlite could sample many sub-populations of diamonds, with no apparent relationship between their physical and chemical characteristics (Deines et al., 1993). It was therefore suggested that the heterogeneity observed in the carbon isotope values was primordial, a signature acquired during Earth's accretion and not subsequently homogenized by mantle convection. While support from this model comes from similarity in the range of $\delta^{13}C$ data obtained from carbon in meteorites and eclogitic diamonds (Deines 1980), it is implausible that ^{13}C depleted primordial heterogeneities should be restricted almost exclusively to metabasaltic diamond substrates. As such, this hypothesis will be excluded from further discussion here, and the focus will be on understanding the arguments for and against the second and third hypotheses.

Fractionation of carbon isotopes, both prior to and during diamond formation, have been a significant part of the discussion surrounding the negative skewness of the eclogitic diamond $\delta^{13}C$ record. Cartigny et al. (1998; 2001) proposed that carbon isotopic fractionation would be driven by the separation of CO_2 from the diamond-forming fluid/melt prior to diamond crystallisation, depleting the fluid/melt in ^{13}C. While this process has not been ruled out, it has been calculated that only very small amounts (<1 %) of the residual fluid/melt reaches a $\delta^{13}C$ value of <-14 ‰, and almost none <-20 ‰ (Smart et al., 2011). So, it is thought unlikely that this process alone can account for the eclogitic diamond $\delta^{13}C$ record.

The case for fractionation processes occurring during diamond growth are based upon equilibrium fractionation factors for carbon isotopes at mantle temperatures, which have been derived from theoretical calculations, experimental determination and empirical measurements (Chacko et al., 2001; Satish-Kumar et al., 2011; Reutsky et al., 2012; 2015; Horita & Polyakov, 2015). Diamond growth through redox reactions (i.e. either the reduction of oxidized carbon species, or the oxidation of reduced

carbon species) produces characteristic $\delta^{13}C$ trends depending on the redox speciation in the fluid/melt (see Cartigny et al., 2014). Diamonds growing from an oxidized fluid/melt, containing CO_2 or CO_3^{2-}, will be offset to lower $\delta^{13}C$ values relative to the source (the exact amount depends on the isotope fractionation factor between the fluid carbon species and diamond), leading to successive enrichment in ^{13}C (Figure 5A, & B). In a fluid-limited system, the resultant diamond population would exhibit a positive skewness in the $\delta^{13}C$ distribution. Conversely, diamonds growing from a reduced fluid/melt containing CH_4, will be initially offset to heavier $\delta^{13}C$ values relative to the source, but in a fluid-limited system will be successively enriched in ^{12}C (Figure 5C). Empirical support for the fractionation hypothesis has come from carbon isotope data obtained from both individual diamonds by SIMS (oxidized fluid/melt – Zedgenizov et al., 2006; Smart et al., 2011; Palot et al., 2013; Mikhail et al., 2014) and diamond populations via bulk analyses (reduced fluid/melt – Thomassot et al., 2007), while the skewness of population distributions have also been discussed (e.g. Deines, 1980; Stachel & Harris, 2009).

Recently, the effectiveness of redox reactions to account for diamond precipitation in peridotitic substrates has been questioned. Luth & Stachel (2014) showed that the redox buffering capacity of peridotitic mantle is insufficient to account for economic quantities of diamonds to form. CHO fluids within depleted peridotitic mantle with compositions near the water-maximum would not contain just one carbon species but both oxidized and reduced (see Figure 1 of Stachel et al., 2017a; Stachel & Luth, 2015). Rayleigh isotope fractionation in multi-component systems is more complex than in systems with a single carbon species; their modeling showed that regardless of the dominant carbon species, diamond always progresses along ^{13}C enrichment paths (Figure 5D). The predicted absence of progression towards more negative $\delta^{13}C$ values even for fluid mixtures dominated by reduced carbon species ($CH_4/CO_2 > 1$), was supported by SIMS data for Marange (Zimbabwe) diamonds that contained CH_4 micro-inclusions yet revealed core-to-rim trends towards heavier $\delta^{13}C$ values (Smit et al., 2016; Stachel et al., 2017a). It is important, however, to highlight the limitations and likely oversimplification of this model. Firstly, it is only truly applicable to harzburgites (in lherzolites and eclogites conditions would be above their solidi, therefore generating more complex melts), and secondly, pure CHO fluids are likely a simplified starting point for the model - they have only been observed as inclusions in

519 diamonds very rarely. Analysis of more typical micro-inclusions containing diamond-
520 forming fluids/melts shows they contain significant proportions of dissolved material
521 (Weiss et al, 2009), which presently are not considered in this model. However,
522 thermodynamical modelling of hydrous solutions in equilibrium with peridotite or
523 eclogite at high pressures and temperatures up to 1000 °C (Sverjensky and Huang,
524 2015; Huang and Sverjensky, 2019) does predict the coexistence of a variety of
525 oxidized and reduced species together with high contents of major oxides.
526
527 The third hypothesis, which invokes recycled carbon as the source of the varied $\delta^{13}C$
528 values, is based around a subducted nature of eclogitic diamond substrates (e.g.
529 Helmstaedt et al., 1972). Altered oceanic crust (AOC; the igneous portion of oceanic
530 crust) shows considerable C isotopic variability. A recent study by Li et al. (2019)
531 suggests the AOC contains two carbon isotopic end-members; (1) a high $\delta^{13}C$ (~0 ‰)
532 carbonate component that forms during low-temperature alteration of the oceanic
533 crust, and (2) isotopically light biogenic carbonate. However, Valley & O'Neill
534 (1981) have shown that very negative $\delta^{13}C$ values can be formed through
535 fractionation (~600 – 800 ^{o}C) and may not necessarily require biogenic origins (see
536 Etiope & Sherwood Lollar, 2013). The occurrence of low $\delta^{13}C$ values in
537 sublithospheric diamonds, whose inclusions have been shown to represent a snapshot
538 of deep subduction (e.g. Deines et al., 1991; Tappert et al., 2005; Brenker et al., 2007;
539 Walter et al., 2011) provides empirical support for this subduction model, along with
540 oxygen isotope analyses of eclogitic garnet inclusions that clearly fall outside the
541 mantle range (Ickert et al., 2013; 2015; Schulze et al., 2013; Burnham et al., 2015).
542 Ickert et al. (2013) interpreted their $\delta^{13}C$ - $\delta^{18}O$ data to represent interaction (not
543 strictly two-component mixing) between fluids carrying '*mantle-like*' carbon (i.e.
544 $\delta^{13}C$ ~-5 ‰) and subducted substrates with non-mantle-like $\delta^{18}O$; the only portion of
545 former AOC that carries enough carbon to not become overwhelmed in its carbon
546 isotope signature by the mantle-derived fluids are highly altered, and hence carbon-
547 enriched, former pillow basalts, where strongly negative $\delta^{13}C$ is invariably associated
548 with high $\delta^{18}O$ ($\delta^{18}O \geq 6$ ‰; Ickert et al. 2013). Li et al. (2019) propose that this link
549 between altered oceanic crust, mantle fluids, diamonds and their inclusions is also
550 capable of explaining the apparent decoupling of C and N isotopes in diamonds
551 (Mikhail et al., 2014; Hogberg et al., 2016).
552

In the present study, we will provide an impartial interrogation of the data reported, along with a comparison with literature data, to evaluate how the above factors fit within the realms of mantle fractionation and subduction models.

Paragenetic Variations in the Diamond Record

The $\delta^{13}C$ mode of both the P- and E-type paragenetic datasets is -5.0 ± 0.5 ‰; 39% of this study's data falls within this tight range (37% for P-type, 41% for E-type) along with 33% of the *total literature data* (obtained through bulk combustion analysis). The proportions of data included increase significantly when only increasing the modal range slightly; 61 % of this study's data fall within -5.0 ± 1.0 ‰ (68% for P-type, 53% for E-type) along with 52% of total literature data; 81 % of this study's data fall within -5.0 ± 2.0 ‰ (90% for P-type, 70% for E-type) along with 73% of literature data. The isotopically light tail observed in the data is clearly confined in this study to the E-type diamonds, with the lowest P-type $\delta^{13}C$ value being only -8.4 ‰.

Our extensive SIMS study (with little or no bias towards individual diamonds that are isotopically heterogeneous and/or depleted in ^{13}C) has produced a dataset that is largely in agreement with the *total literature database* obtained through bulk combustion analyses. This provides significant support to the utility of bulk $\delta^{13}C$ data. Bulk combustion averages out internal variations from multiple growth layers, potentially missing out on reporting the full range of carbon isotope values present. However, given that 66 % of our samples showed <1 ‰ internal $\delta^{13}C$ variation, with 86 % <2 ‰ and 96 % <3 ‰, it is clear that the bulk analysis of diamond fragments will generally yield a good approximation of their carbon isotopic composition.

While both the P and E-type datasets have a mode around -5 ‰, it is clear from the population statistics, and from previous studies, that eclogitic diamonds show more variation and a greater prevalence of ^{13}C depleted isotopic values. The standard deviation about the mean for the E-type data set (±2.5 ‰) is more than double that for the P-type data (±1.1 ‰) and the E-type distribution is skewed to lower $\delta^{13}C$ values (-1.3; Pearson's Coefficient of Skewness, see Table 3) compared to a negligible

positive skewness of the P-type data (0.2). This is broadly in keeping with the literature data. The P-type literature data are, however, far more tightly distributed around the -5 ‰ mode and nearly 34 % of published E-type $\delta^{13}C$ data fall below -10 ‰ (only ~16 % in this study), compared to only around 1 % of P-type diamonds (0 % in this study). The average variation observed in individual P-type diamonds in this study is 0.85 ‰, compared to a value of 1.53 ‰ in the E-type diamonds (which includes the 4 samples with highly negative cores). Therefore, E-type diamonds typically do exhibit more internal variation in $\delta^{13}C$ values compared with P-type diamonds.

The E-type dataset's distribution has a more bimodal appearance than the literature data (see Figure 4 of Cartigny et al., 2014). The main reason for this is the over-representation of data from Argyle. With its prominently ^{13}C-depleted distribution (68 % of the Argyle data in this study is lower than -9 ‰, for the literature it is ~86 %) it is over-represented in this study (18 %) compared to the literature (~9 %). However, Argyle is not the only deposit in the world to have a signature of predominantly ^{13}C depleted diamond carbon. Guaniamo (Venezuela), Jagersfontein (South Africa), Dachine (French Guiana) and Jericho (Canada), all have population modes that are even lower than seen in Argyle diamonds (see Figure 5 of Cartigny et al. (2014) and references therein), so the bimodality may persist even if the dataset is expanded.

Isotopic Trends within Individual Diamonds

The advantage of *in situ* SIMS analysis of diamond is the power to reveal isotopic core-to-rim trends within individual samples, which can provide evidence of Rayleigh fractionation processes and potentially reveal the speciation of the diamond-forming fluids. Diamond core-to-rim fractionation trends have been observed in several diamond suites (Zedgenizov et al., 2006; Thomassot et al., 2007; Smart et al., 2011; Palot et al., 2013; Wiggers de Vries et al., 2013; Petts et al., 2015; Smit et al., 2016; 2019a), however these trends are typically associated with small overall $\delta^{13}C$ variations <3 ‰. When we consider the data from the present study, there are no convincing trends observed in any of the 144 samples examined in detail. Figure 6

617 shows typical traverses observed in the diamonds studied here, with non-systematic
618 variations in $\delta^{13}C$ and/or N contents. Two thirds of the samples analysed showed <1
619 ‰ variation in $\delta^{13}C$ (one third <0.5 ‰). Overall, our data set shows that diamonds
620 with recognizable fractionation trends are generally very rare. Despite a number of
621 publications reporting clear fractionation trends (see above), our globally
622 representative sample set documents that diamonds with systematic and significant
623 co-variations in $\delta^{13}C$ and [N] are the exception rather than the rule. This suggests that
624 diamond is a more passive recorder of changing $\delta^{13}C$ rather than being the cause of
625 $\delta^{13}C$ variability. The agreement in the modes between the bulk analytical data and our
626 *in situ* data strongly supports this view and we conclude that significant closed system
627 isotopic fractionation did not operate for the majority of individual growth events.
628 This implies that diamond growth typically occurs in temporally and spatially
629 localized systems with high excess of carbon in the fluid, i.e. relative to the mass of
630 growing diamonds.

631 This conclusion has important implications for the discussion surrounding the
632 syngeneity or protogeneity of inclusions in diamond (see Nestola et al. (2017) and
633 references therein), and the ramifications on diamond growth ages obtained from
634 these inclusions. If diamond inclusions are protogenetic, then in a process with high
635 fluid:rock ratios, the likelihood of the inclusions being isotopically reset at the time of
636 diamond formation is high. This would lead to inclusion ages being representative of
637 the diamond growth event (i.e. being synchronous), irrespective of whether they are
638 syngenetic. Although detailed study has shown that mineral inclusion size and
639 residence temperature play an important role (Nestola et al., 2019). Isotopic resetting
640 has been categorically shown for sulphide inclusions from Zimmi (Smit et al., 2016;
641 2019b) where inclusions in three different diamonds provide the same isochron ages,
642 yet their Re-Os and sulphur isotopes both show that the sulphides were existing in the
643 lithosphere prior to the diamond formation event.

644 The work of Stachel et al. (2017a) on Rayleigh isotopic fractionation in
645 multicomponent systems (RIFMS) during isochemical precipitation showed that in
646 water-maximum fluids within harzburgitic domains, fractionation could only account
647 for variations of <1 ‰. This is in keeping with the lack of significant variation seen in
648 the peridotitic diamonds of this and former studies, but is not the only potential

649 explanation (see following paragraph). In the simplest water-maximum RIFMS
650 model, with only CO_2 and CH_4 as carbon-bearing species, the fluid speciation ($X_{[CO_2]}$
651 = $CO_2/[CO_2+CH_4]$) and the dependent variable oxygen fugacity exert a strong control
652 on the carbon isotope composition of the precipitated diamond, irrespective of growth
653 mode (Figure 5D). For both isochemical and wall-rock buffered redox scenarios, the
654 carbon isotope composition of the first precipitated diamond only depends on the
655 $X_{[CO_2]}$ of the fluid and its assumed starting composition. Carbon isotopic evolution of
656 the fluid would differ depending on whether diamond formation occurs isochemically
657 or through wall rock-buffered redox reactions and whether the system is fluid-limited
658 or not. However, the variation is limited as the effective fractionation factor is the
659 weighted average of the factors of CH_4 and CO_2, which oppose each other. As both
660 species are consumed in equal amount the variation in fO_2 is also limited. The model
661 shows that the first precipitated diamond varies by 3.7 ‰ in $\delta^{13}C$ over a range of
662 $X_{[CO_2]}$ values from 0.9 to 0.1, which corresponds to a total increase in Δ log fO_2
663 (FMQ) of only about 0.8 log units. Assuming diamond-forming fluids with a constant
664 mantle-like $\delta^{13}C$ value of -5 ‰, it is, therefore, possible to account for the principal
665 mode of -5 ± 1 ‰ in the global harzburgitic diamond record with a variation in fO_2 of
666 just 0.4 log units, based on modelling of diamond formation at constant depth along a
667 geotherm.
668
669 The water-maximum fluids model is somewhat simplified (see earlier discussion in
670 *Carbon Isotope Systematics* section). However, as more realistic thermodynamic
671 models of subsolidus fluids also predict the presence of CO_2, carbonates and more
672 reduced organic species (e.g. Sverjensky and Huang, 2015; Tiraboschi et al., 2018)
673 the conclusions of the above modelling should still be applicable. If dissolved
674 carbonate joins the assemblage, it should act to further limit the fractionation. While
675 subsolidus fluids are expected in harzburgitic rocks along the 40 mW/m^2 model
676 geotherm, lherzolitic and eclogitic mantle would be above the hydrous solidus. Saline
677 and carbonatitic melts similar to the high-density fluids trapped in fibrous diamonds
678 may also infiltrate all these rocks. Still, as long as the fluids and melts carry both
679 oxidized carbonate and/or CO_2 together with reduced species, fractionation is
680 expected to be rather limited.
681

682 If diamond precipitation has only a limited ability to fractionate the carbon isotopic
683 composition of mantle fluids, and if their isotopic composition reflects that of the
684 fluid to within ±1 ‰, then, the pronounced mode of diamond $\delta^{13}C$ values through
685 time at about -5 ‰ leads to the conclusion that the speciation and consequently
686 oxygen fugacity of diamond forming mantle fluids has been relatively consistent since
687 ~3.5 Ga. This also means that the deep (sublithospheric?) mantle has provided fluids
688 with near constant carbon speciation for the last 3.5 billion years.
689
690 At present there is no single model that is widely accepted, to account for the
691 increased variability of $\delta^{13}C$ values in eclogitic diamonds. The cause of this greater
692 variability in the $\delta^{13}C$ record of eclogitic diamonds may reflect either (1) diamond-
693 forming fluids with significantly more varied carbon characteristics - stemming from
694 subducted material containing highly variable biogenic and/or abiogenic carbon
695 sources, or (2) a growth environment more prone to significant isotopic fractionation
696 between the diamond and fluid/melt, or (3) a combination of both of these scenarios.
697 We note that an isotopically light carbon surface reservoir was available on Earth for
698 recycling to the mantle depths of diamond growth since 3.5 Ga (e.g. Des Marais,
699 2001) removing the need to produce this signal solely in the mantle by fractionation.
700
701
702 *The Diamond Record Through Time*
703
704 Figure 7 places the diamond carbon isotope record into a chronological context using
705 data from this study and the *dated literature data*. The restricted nature of peridotitic
706 $\delta^{13}C$ values (as discussed previously) appears consistent through time, as does the
707 occurrence of isotopically light carbon (< -10 ‰) in eclogitic diamonds. However, the
708 mode of eclogitic $\delta^{13}C$ values is still at -5 ‰, consistent with that of the peridotitic
709 diamonds. Isotopically light carbon only represents a very small proportion of the
710 data; 6 % of the data from this study and 10 % of the *dated literature data* (excluding
711 the SIMS data) shown in Figure 7. The tail towards ^{13}C-depleted carbon in the
712 eclogitic diamonds also shows no signs of systematic variation through time (Figure
713 7), with its first occurrence in the record from 3 Ga onwards. With the oldest eclogitic
714 diamonds being tied to the onset of plate tectonics (Helmstaedt et al., 2010; Shirey &
715 Richardson, 2011), if the low $\delta^{13}C$ carbon signature is related to a biogenic carbon

716 contribution in altered oceanic crust (Li et al., 2019), this would imply that this
717 contribution, with respect to both amount and $\delta^{13}C$ values, has been fairly consistent
718 through 3 Ga. This is supported by the Precambrian marine carbonate isotope
719 database (Shields and Veizer, 2002). But the data in Figure 7 also shows that
720 isotopically light carbon, the potential key biomarker in altered oceanic crust, was not
721 recycled to mantle keel depths as extensively and consistently before 3 Ga as it was
722 after 3 Ga. Whether this was due to a geodynamic cause such as the absence of
723 eclogite recycling or a biologic cause such as the absence of biogenic components
724 deep in the oceanic crust or both is unknown. The important point is that the onset of
725 the temporal appearance of deeply-sourced, isotopically light carbon had only been
726 previously inferred from mineral inclusion paragenesis and general E-Type diamond
727 carbon isotope histograms. For the first time, this study has established the onset and
728 persistence of deep recycling of potentially biogenic carbon in the rock record by
729 direct analysis of the geochronologically dated carbon itself.
730
731 Looking at the $\delta^{13}C$ and N data together provides additional insight into potential
732 variations through time. Here we used multidimensional scaling (MDS) and principal
733 component analysis (PCA) to better visualise similarities and differences in the data.
734 MDS was only carried out on the $\delta^{13}C$ data as a function of their locations, while PCA
735 was carried out on the combined $\delta^{13}C$ and [N] datasets (see Supplementary Materials
736 for detailed information about this data processing methodology).
737
738 For the P-type data, MDS of the $\delta^{13}C$ values shows strong overlap between the
739 various populations with one exception (Figure 8a). There is clear discrimination
740 between Wawa and the two older diamond growth events at Diavik and De Beers
741 Pool (Figure 8a), while the three younger growth events (Venetia, Udachnaya and
742 Ellendale) exhibit more spread on the *x*-axis and overlap with all three of the older
743 populations. This observation is repeated in the PCA plot (Figure 8b). Despite N
744 concentration being the most significant variable in creating the spread in the data (i.e.
745 it is weighted most heavily in principal component 1), the discrimination caused by
746 just the $\delta^{13}C$ values is still retained in the PCA. This discrimination is the result of
747 $\delta^{13}C$ data for Wawa diamonds having a mode at -4 ‰ and its distribution having the
748 most positive skewness of all the P-type populations, while the older diamonds from
749 Diavik and De Beers Pool have strong modes at -5 ‰ and distributions with more

750 negative skewness. Despite this one minor difference in the data from 6 populations,
751 the PCA and MDS strongly reinforce the findings from the earlier interrogation of the
752 data (Figures 2 and 7), that there is no significant variation in $\delta^{13}C$ with geological
753 time for peridotitic diamonds.
754
755 Despite diamond growth at Wawa only being constrained by a minimum age, it is
756 interesting to consider the data in the broader context of the Superior Craton on which
757 the diamonds occur. Diamonds from the Renard (Quebec), Kyle Lake and
758 Attawapiskat (Ontario) kimberlites of the eastern and central Superior Craton,
759 respectively, show a temporal variation in $\delta^{13}C$. The Neoproterozoic Renard and T1
760 (Kyle Lake) kimberlites, along with Wawa (Neoarchean), carry diamond populations
761 with a mode in $\delta^{13}C$ of -4 ‰ (Hunt et al., 2012; Smit et al., 2014; Stachel et al., 2006)
762 while the Jurassic U2 (Attawapiskat) and Victor pipes exhibit a mode of -5 ‰ (Smit
763 et al., 2014; Stachel et al., 2017b). Between the emplacement of the Kyle Lake and
764 Attawapiskat kimberlites, the southern Superior craton experienced the major
765 Midcontinent Rift event at 1.1 Ga, which is considered to have been diamond-
766 destructive beneath the Attawapiskat area (Smit et al., 2014; Aulbach et al., 2018;
767 Stachel et al. 2018). Globally, our data show no discernible variation of mantle carbon
768 through time; yet, it is clear that detailed studies on the regional / craton scale have
769 the potential to reveal subtle temporal variations. However, it is not possible to
770 discern whether this change beneath the Superior Craton is caused by a small change
771 in the starting carbon isotopic composition, or the carbon speciation (and the
772 dependent variable oxygen fugacity) of the diamond-forming fluid.
773
774 While the MDS and PCA plots of the E-type data show more spread (Figure 9a & b)
775 than their corresponding P-type plots, the data from Argyle appear to be a slight
776 outlier. Even though the Argyle data are by no means fully discrete from any other
777 data set, these are the only diamonds with data entirely outside the main cluster. Since
778 the earliest proposals of subducted organic matter playing a role in diamond formation
779 (Sobolev & Sobolev, 1980; Milledge et al., 1983), Argyle has been the primary case
780 study to support this model (e.g., Jaques et al., 1989; Stachel et al., 2018) with its
781 dominance of eclogitic inclusions (~90%) and the normal distribution of $\delta^{13}C$ data
782 around a mode of -11 ‰. Detailed study of the diamonds and their inclusions have led
783 to the conclusion that eclogitic diamond growth predominantly occurred at unusually

784 high temperatures (~1250 – 1400 ^{o}C), indicating a depth at the very base of the
785 lithospheric mantle (Bulanova et al., 2018; Stachel et al., 2018). Recent noble gas
786 analyses also support a subducted origin for the Argyle eclogitic diamonds which
787 typically have low R/Ra values (<0.5; where R/Ra=^{3}He/^{4}He$_{sample}$ / ^{3}He/^{4}He$_{air}$) with the
788 noble gas subduction signatures focused at the base of the lithosphere, suggesting less
789 extensive fluid migration and interaction at higher levels with the sub-continental
790 lithospheric mantle (Timmerman et al., 2019b). Argyle reflects a strong case for
791 subduction-related diamond growth, but what potentially makes Argyle unique is the
792 amount of subducted carbon involved. Whether there was extensive mixing at greater
793 than average depths, of a large amount of isotopically light carbon with either mantle
794 carbon or isotopically heavier subducted carbonates, it created a fairly homogenized
795 diamond-forming fluid with an intermediate δ^{13}C signature. This contrasts with the
796 more common observation of a minor isotopically light (~-25 ‰) δ^{13}C signature
797 coupled with a dominant *mantle-like* (~-5 ‰) δ^{13}C signature.
798
799 There are two deposits, Orapa and Jwaneng, in our E-type dataset that have multiple
800 dated diamond growth events. This provides some insights into potential variations of
801 carbon through time within small sections of the mantle. The PCA of Orapa data
802 subdivided by age (Figure 9c) reveals some discrimination between the
803 subpopulations, with potential mixing between two end-members. The 2.1 Ga
804 samples have some overlap with the 3 Ga samples, but largely fall in a distinct group,
805 while the 1 Ga samples seemingly spread between the two. Potential endmember (1)
806 has more negative δ^{13}C values (-8 to -12 ‰) coupled with lower nitrogen
807 concentrations (<400 ppm), while endmember (2) has more *mantle-like* δ^{13}C values (-
808 4 to -8 ‰) and higher nitrogen concentrations (>400 ppm). This indicates potential
809 variation in the source of diamond forming fluids beneath Orapa through time, in
810 agreement with a similar conclusion by Timmerman et al. (2017) based upon carbon
811 and strontium isotope analyses of Orapa and Letlhakane diamonds. Although
812 Timmerman et al. (2017) discerned three potential endmembers, it is important to bear
813 in mind that only 2 of the 13 Orapa samples in this present study did not show
814 evidence of containing multiple growth events. Therefore, it is possible that the dating
815 of individual growth zones combined with detailed SIMS analyses may reveal a
816 clearer distinction as to identifying the potential sources of carbon through time at
817 Orapa. Interestingly, the PCA and MDS processing of the Jwaneng data reveal no

818 such subdivision with age. In fact, Orapa, and nearby Letlhakane, (Timmerman et al.,
819 2017) are the only deposits where a variation in the diamonds' carbon isotope record
820 with time has been documented (N.B. this excludes the consideration of fibrous and
821 polycrystalline diamond growth events, as well as those without multiple defined ages
822 at a single location). Despite the subtle variations seen at Orapa and the offset to
823 lower $\delta^{13}C$ seen at Argyle, the remaining E-type data reveal no systematic variations
824 in $\delta^{13}C$ through time on a global scale. This applies to the occurrence of both the $\delta^{13}C$
825 mode of -5 ‰ as well as the skewness of distributions to the more negative $\delta^{13}C$
826 values.
827
828 *Summary*
829
830 This comprehensive statistical interrogation of the diamond record for carbon isotope
831 values and nitrogen content through time revealed that, despite potential local
832 fluctuations, in general there is no systematic variation with time in the mantle carbon
833 isotope record over 3 billion years. The mode $\delta^{13}C$ of peridotitic diamonds has been at
834 -5 (± 2) ‰ since the earliest diamond growth ~3.5 Ga, and it is also observed in the
835 eclogitic diamond record since ~3 Ga. The skewed distribution of the $\delta^{13}C$ in eclogitic
836 diamonds to more negative values is also consistent through time, with no discernible
837 global trends apparent. However the onset of recycled, isotopically light C that was
838 suggested from Sm-Nd and Re-Os data on dated inclusions (Shirey & Richardson,
839 2011) is corroborated by a complete C isotope dataset.
840
841 On a local level, it is clear that individual deposits can have carbon isotope
842 distributions that are subtly (Wawa) or more obviously (Argyle) different to the global
843 norm. There is also scope to reveal variations over time in the diamond populations at
844 a single locality (Orapa). What is surprising, however, is that these variations are not
845 more common. The $\delta^{13}C$ range observed in eclogitic diamonds is a reflection of
846 complex and varied growth environments, potentially involving more significant
847 amounts of fractionation, and/or multiple, isotopically distinct carbon sources. A
848 marked divergence from the global norm is seemingly very limited, with Argyle being
849 the most notable (and most studied) exception. The more limited $\delta^{13}C$ range observed
850 in peridotitic diamond populations likely reflects a simpler growth environment,
851 associated with the influx of mantle derived CHO-fluids, with less inherent variability

compared to subduction-related scenarios. This more stable and consistent environment potentially allows for more subtle variations in the $\delta^{13}C$ data to be attributed to minor shifts in the chemistry of the diamond-forming fluids (e.g. Wawa, Kyle Lake and the Attawapiskat diamonds on the Superior Craton).

Despite this potential for variation and heterogeneity, mantle carbon as recorded by diamond has remained remarkably consistent over the course of Earth's history.

Conclusions

This study has utilized detailed *in situ* SIMS analyses of a large collection of diamonds with established formation ages, providing insight into the deep carbon record over a 3.5 Ga time period, from various cratons worldwide. This work reveals a lack of discernible systematic variations in the global carbon isotope composition of Earth's mantle through time as recorded by peridotitic diamonds. Despite eclogitic diamonds having more varied C isotopic values on an individual crystal basis, on a deposit-scale basis and globally, their C isotopic variability is generally consistent overall and also lacks any discernible systematic temporal variation. While there are clear examples in both the P-type (e.g. Wawa) and E-type (e.g. Argyle) populations of individual deposits whose carbon records sit outside the global norm, the overall consistency of the diamond record is remarkable. Examples of temporal variation within individual diamond deposits (E-type diamond record at Orapa; Timmerman et al., 2017) and on the craton-scale (Archean versus Neoproterozoic P-type diamonds from the Superior Craton) do exist but are the exception. Despite these anomalies, the global $\delta^{13}C$ diamond record for diamond growth in both peridotitic and eclogitic substrates is remarkably consistent through time.

The fact that the *in situ* dataset reported here provides very good agreement with the global "bulk" diamond record is a very important finding, which confirms earlier combustion studies of internal heterogeneity (Galimov, 1984; Cartigny et al., 2004; Mikhail et al., 2014). Despite single combustion analyses not recording internal heterogeneity within individual diamonds, the global bulk dataset is representative of the diamond record and interpretations based upon it have a solid foundation. A key reason for this agreement is that the typical variation of $\delta^{13}C$ values in individual

886 diamond fragments sampled in this study is small, with two thirds of the samples
887 varying by <1 ‰. Additionally, no clear fractionation trends were observed in any of
888 the diamonds studied here, indicating that fluid-limited conditions during diamond
889 growth are very rare and proportionally over-represented in the literature. Instead,
890 diamond growth appears to typically occur in systems with excess of carbon in the
891 fluid, precluding significant Rayleigh fractionation during continued diamond
892 crystallization. A significant implication of this is that inclusions are very likely to be
893 isotopically reset at the time of diamond formation in a fluid-rich environment, either
894 through fluid-assisted equilibration/diffusion or more extensive partial melting,
895 meaning that the radiogenic isotope systematics of diamond inclusions reflect
896 formation ages irrespective of the inclusions being syngenetic or protogenetic with
897 respect to diamond growth (Smit et al., 2016; 2019b; Nestola et al., 2019).
898
899 The global literature diamond database has a remarkably consistent mode in $\delta^{13}C$ at -5
900 ‰ over 3.5 Ga. While the majority of samples in the database were not directly dated,
901 this present study has provided the temporal context to show that this mode in the
902 $\delta^{13}C$ is also consistent through time. Focusing on peridotitic diamonds that mostly
903 would have grown under subsolidus conditions (Stachel & Luth, 2015), the data from
904 this study show a tight grouping around this mode (90% fall within -5 ± 2 ‰), which
905 is also consistent with literature data. Modelling of this dataset through growth from
906 water-maximum CHO fluids reveals that this range can be accounted for by only a
907 small variation in the carbon speciation of the fluid (0.4 log units), which in turn
908 reflects a remarkably consistent redox state of these diamond-forming fluids for 3.5
909 Ga.
910
911 Despite eclogitic diamond growth not necessarily occurring in a subsolidus
912 environment (Stachel & Luth, 2015), the E-type diamond record also has a consistent
913 $\delta^{13}C$ mode of -5 ‰ (70% of data fall within -5 ± 2 ‰). Total $\delta^{13}C$ variation in
914 individual diamonds is generally minor (typically <2 ‰); when the internal variation
915 is larger, it is often occurring due to multiple discrete growth events. Even when
916 carbon isotope fractionation trends have been recorded in some rare diamond
917 examples, the total variation has always been <3 ‰. This suggests that the
918 environment for diamond growth is not conducive to generating significant variations
919 through fractionation processes alone. In view of the strong negative skewness of the

E-type diamond record, down to values of ~-40 ‰ (De Stefano et al., 2009), this range of $\delta^{13}C$ values is considered to be predominantly the result of variations in the carbon signal of the primary fluids/melt. The subducted nature of eclogites, containing some isotopically light abiogenic and/or biogenic carbon, is the prevalent model to explain the cause of the negative skew in eclogitic diamond $\delta^{13}C$ values (Sobolev & Sobolev, 1980; Milledge et al., 1983; Kirkley et al., 1991).

The earliest eclogitic diamonds have been tied to the onset of subduction and plate tectonics (Helmstaedt et al., 2010; Shirey & Richardson, 2011). The appearance of isotopically light carbon at 3 Ga and its persistence in the eclogitic paragenesis after that time affirms a secular change in recycled carbon at this time. If this is indeed the case, then ultimately the net effect of subduction has not altered the ambient signal of the mantle's carbon record. Whether this is due to the net carbon isotopic composition of a subducted plate being about -5 ‰ (Shilobreeva et al., 2011), or the fact that recycled carbon is just a very minor contribution in the overall mantle carbon budget, remains to be proven.

Acknowledgements

We thank the Deep Carbon Observatory (DCO) for funding the Diamonds and the Mantle Geodynamics of Carbon Group (DMGC) and the research reported in this paper. In particular, Erik Hauri was a long-standing enthusiastic supporter of diamond research within the DCO. Discussions with Andrew Steele among others were an important catalyst for this work. DH wishes to personally thank TS, FN and DGP for their continued support prior to and throughout this project. Many of the diamonds studied here were donated to JWH by the Diamond Trading Company (a member of the De Beers group of Companies); this generosity is greatly appreciated. Suzette Timmerman is thanked for providing her SIMS data for the literature database. Sami Mikhail and an anonymous reviewer, as well as editor Dmitri Ionov, are thanked for their comments which helped to improve the manuscript. TS acknowledges funding through a Natural Sciences and Engineering Research Council of Canada Discovery grant and through the Canada Research Chairs program.

References

Appleyard, C. M., Viljoen, K. S., & Dobbe, R. (2004). A study of eclogitic diamonds and their inclusions from the Finsch kimberlite pipe, South Africa. Lithos, 77(1-4), 317-332.

Aulbach S. and Stagno V. (2016) Evidence for a reducing Archean ambient mantle and its effects on the carbon cycle. Geology 44, 751-754.

Aulbach S. and Viljoen K. S. (2015) Eclogite xenoliths from the Lace kimberlite, Kaapvaal craton: From convecting mantle source to palaeo-ocean floor and back. Earth & Planetary Science Letters, 431, 274–286.

Aulbach, S., Creaser, R. A., Stachel, T., Heaman, L. M., Chinn, I. L., & Kong, J. (2018). Diamond ages from Victor (Superior Craton): Intra-mantle cycling of volatiles (C, N, S) during supercontinent reorganisation. Earth and Planetary Science Letters, 490, 77-87.

Aulbach, S., Stachel, T., Creaser, R.A., Heaman, L.M., Shirey, S.B., Muehlenbachs, K., Eichenberg, D. & Harris, J.W. (2009). Sulphide survival and diamond genesis during formation and evolution of Archaean subcontinental lithosphere: A comparison between the Slave and Kaapvaal cratons. Lithos, 112, 747-757.

Aulbach, S., Woodland, A. B., Vasilyev, P., Galvez, M. E., & Viljoen, K. S. (2017). Effects of low-pressure igneous processes and subduction on Fe3+/ΣFe and redox state of mantle eclogites from Lace (Kaapvaal craton). Earth and Planetary Science Letters, 474, 283-295.

Ballhaus, C. and Frost, B. R. (1994). The generation of oxidized CO2-bearing basaltic melts from reduced CH4-bearing upper mantle sources. Geochimica et Cosmochimica Acta, 58(22), 4931-4940.

Berry A. J., Danyushevsky L. V., O'Neill H. S. C., Newville M. & Sutton S. R. (2008) Oxidation state of iron in komatiitic melt inclusions indicates hot Archaean mantle. Nature 455(7215), 960–963.

Bottinga, Y. (1969). Calculated fractionation factors for carbon and hydrogen isotope exchange in the system calcite-carbon dioxide-graphite-methane-hydrogen-water vapor. Geochimica et Cosmochimica Acta, 33(1), 49-64.

Brenker, F.E., Vollmer, C., Vincze, L., Vekemans, B., Szymanski, A., Janssens, K., Szaloki, I., Nasdala, L., Joswig, W. & Kaminsky, F. 2007. Carbonates from the lower part of transition zone or even the lower mantle. Earth and Planetary Science Letters, 260(1-2), 1-9.

Bulanova, G. P., Pearson, D. G., Hauri, E. H., & Griffin, B. J. (2002). Carbon and nitrogen isotope systematics within a sector-growth diamond from the Mir kimberlite, Yakutia. Chemical Geology, 188(1-2), 105-123.

Bulanova, G.P., Speich, L., Smith, C.B., Gaillou, E., Kohn, S.C., Wibberley, E., Chapman, J.G., Howell, D., & Davy, A.T. (2018), The unique nature of Argyle fancy diamonds: Internal structure, paragenesis, and reasons for color. Society of Economic Geologists, Special Publication 20, 169–190.

Burnham, A. D., Thomson, A. R., Bulanova, G. P., Kohn, S. C., Smith, C. B., & Walter, M. J. (2015). Stable isotope evidence for crustal recycling as recorded by superdeep diamonds. Earth and Planetary Science Letters, 432, 374-380.

Canil D. (1997) Vanadium partitioning and the oxidation state of Archaean komatiite magmas. Nature 389(6653), 842–845.

Canil D. and Fedortchouk Y. (2001) Olivine-liquid partitioning of vanadium and other trace elements, with applications to modern and ancient picrites. Canadian Mineralogist, 39, 319–330.

Cartigny, 2005. Stable isotopes and the origin of diamond. Elements, 1, 79-84.

Cartigny, P., Harris, J. W., & Javoy, M. (1998). Eclogitic diamond formation at Jwaneng: no room for a recycled component. Science, 280(5368), 1421-1424.

Cartigny, P., Harris, J. W., & Javoy, M. (2001). Diamond genesis, mantle fractionations and mantle nitrogen content: a study of δ13C–N concentrations in diamonds. Earth and Planetary Science Letters, 185(1-2), 85-98.

Cartigny, P., Stachel, T., Harris, J. W., & Javoy, M. (2004). Constraining diamond metasomatic growth using C-and N-stable isotopes: examples from Namibia. Lithos, 77(1-4), 359-373.

Cartigny, P., Palot, M., Thomassot, E., & Harris, J. W. (2014). Diamond formation: a stable isotope perspective. Annual Review of Earth and Planetary Sciences, 42, 699-732.

Chacko, T., Cole, D. R., & Horita, J. (2001). Equilibrium oxygen, hydrogen and carbon isotope fractionation factors applicable to geologic systems. Reviews in mineralogy and geochemistry, 43(1), 1-81.

De Vries, D. W., Pearson, D. G., Bulanova, G. P., Smelov, A. P., Pavlushin, A. D., & Davies, G. R. (2013). Re–Os dating of sulphide inclusions zonally distributed in single Yakutian diamonds: Evidence for multiple episodes of Proterozoic formation and protracted timescales of diamond growth. Geochimica et Cosmochimica Acta, 120, 363-394.

Deines, P. (1980). The carbon isotopic composition of diamonds: relationship to diamond shape, color, occurrence and vapor composition. Geochimica et Cosmochimica Acta, 44, 943-961.

Deines, P. (2002). The carbon isotope geochemistry of mantle xenoliths. Earth-Science Reviews, 58(3-4), 247-278.

Deines, P., Harris, J. W., & Gurney, J. J. (1991). The carbon isotopic composition and nitrogen content of lithospheric and asthenospheric diamonds from the Jagersfontein and Koffiefontein kimberlite, South Africa. Geochimica et Cosmochimica Acta, 55(9), 2615-2625.

Deines, P., Harris, J. W., & Gurney, J. J. (1993). Depth-related carbon isotope and nitrogen concentration variability in the mantle below the Orapa kimberlite, Botswana, Africa. Geochimica et Cosmochimica Acta, 57(12), 2781-2796.

Delano J. W. (2001) Redox history of the Earth's interior since ~3900 Ma: implications for prebiotic molecules. Origins of Life and Evolution of the Biosphere, 31(4–5), 311–341.

Des Marais, D. (2001). Isotopic Evolution of the Biogeochemical Carbon Cycle During the Precambrian. Reviews in Mineralogy and Geochemistry 43(1), 555 578.

Donnelly, C. L., Stachel, T., Creighton, S., Muehlenbachs, K., & Whiteford, S. (2007). Diamonds and their mineral inclusions from the A154 South pipe, Diavik Diamond Mine, Northwest territories, Canada. Lithos, 98(1-4), 160-176.

Fitzsimons, I. C. W., Harte, B., Chinn, I. L., Gurney, J. J., & Taylor, W. R. (1999). Extreme chemical variation in complex diamonds from George Creek, Colorado: a SIMS study of carbon isotope composition and nitrogen abundance. Mineralogical Magazine, 63(6), 857-878b.

Foley, S. F. (2010). A reappraisal of redox melting in the Earth's mantle as a function of tectonic setting and time. Journal of Petrology, 52(7-8), 1363-1391.

Frost, D. J. and McCammon, C. A. (2008). The redox state of Earth's mantle. Annual Reviews of Earth and Planetary Sciences, 36, 389-420.

Galimov, E. M. (1984). The relation between formation conditions and variations in isotope composition of diamonds. Geochemistry International, 22(1), 118-141.

Galimov E.M. (1991) Isotope fractionation related to kimberlite magmatism and diamond formation. Geochimica et Cosmochimica Acta, 55, 1697-1708.

Gurney, J.J., Helmstaedt, H.H., Richardson, S.H., Shirey, S.B., 2010. Diamonds through Time. Economic Geology, 105(3), 689-712.

Harte, B. and Otter, M. (1992). Carbon isotope measurements on diamonds. Chemical Geology 101(1-2), 177-183.

Harte, B., Fitzsimons, I. C. W., Harris, J. W., & Otter, M. L. (1999). Carbon isotope ratios and nitrogen abundances in relation to cathodoluminescence characteristics for some diamonds from the Kaapvaal Province, S. Africa. Mineralogical Magazine, 63(6), 829-856.

Hauri, E. H., Wang, J., Pearson, D. G., & Bulanova, G. P. (2002). Microanalysis of δ13C, δ15N, and N abundances in diamonds by secondary ion mass spectrometry. Chemical Geology, 185(1-2), 149-163.

Hazen, R.M. and Schiffries, C.M. (2013). Why deep Carbon? Reviews in Mineralogy & Geochemistry, 75, 1-6.

Helmstaedt, H., Anderson, O. L., & Gavasci, A. T. (1972). Petrofabric studies of eclogite, spinel- Websterite, and spinel- lherzolite Xenoliths from kimberlite- bearing breccia pipes in southeastern Utah and northeastern Arizona. Journal of Geophysical Research, 77(23), 4350-4365.

Helmstaedt, H. H., Gurney, J. J., & Richardson, S. H. (2010). Ages of cratonic diamond and lithosphere evolution: constraints on Precambrian tectonics and diamond exploration. The Canadian Mineralogist, 48(6), 1385-1408.

Hibbert K. E. J., Williams H. M., Kerr A. C., & Puchtel I. S. (2012) Iron isotopes in ancient and modern komatiites: evidence in support of an oxidised mantle from Archean to present. Earth & Planetary Science Letters, 321–322, 198–207.

Hogberg, K., Stachel, T., & Stern, R. A. (2016). Carbon and nitrogen isotope systematics in diamond: Different sensitivities to isotopic fractionation or a decoupled origin?. *Lithos*, *265*, 16-30.

Horita, J. and Polyakov, V. B. (2015). Carbon-bearing iron phases and the carbon isotope composition of the deep Earth. Proceedings of the National Academy of Sciences, 112(1), 31-36.

Howell, D., O'Neill, C. J., Grant, K. J., Griffin, W. L., O'Reilly, S. Y., Pearson, N. J., Stern, R. A. & Stachel, T. (2012). Platelet development in cuboid diamonds: insights from micro-FTIR mapping. Contributions to Mineralogy and Petrology, 164(6), 1011-1025.

Howell, D., Griffin, W.L., Piazolo, S., Say, J.M., Stern, R.A., Stachel, T., Nasdala, L., Rabeau, J.R., Pearson, N.J. & O'Reilly, S.Y., (2013). A spectroscopic and carbon-isotope study of mixed-habit diamonds: Impurity characteristics and growth environment. American Mineralogist, 98(1), pp.66-77.

Huang, F. and Sverjensky, D.A. (2019). Extended Deep Earth Water Model for predicting major element mantle metasomatism. Geochimica et Cosmochimica Acta, 254, 192-230.

Hunt, L., Stachel, T., McCandless, T.E., Armstrong, J., & Muelenbachs, K. (2012). Diamonds and their mineral inclusions from the Renard kimberlites in Quebec. Lithos, 142, 267-284.

Ickert, R. B., Stachel, T., Stern, R.A., & Harris, J.W. (2013). Diamond from recycled crustal carbon documented by coupled δ18O–δ13C measurements of diamonds and theirinclusions. Earth and Planetary Science Letters, 364, 85-97.

Ickert, R. B., Stachel, T., Stern, R. A., & Harris, J.W. (2015). Extreme 18O-enrichment in majorite constrains a crustal origin of transition zone diamonds. Geochemical Perspectives Letters, 1(1), 65-74.

Jaques, A.L., Hall, A.E., Sheraton, J., Smith, C.B., Sun, S.-S., Drew, R.M., Foudoulis, C., & Ellingsen, K. (1989). Composition of crystalline inclusions and C-isotopic composition of Argyle and Ellendale diamonds. In: Ross, J., et al. (Eds.), Kimberlites and Related Rocks, Their Crust/Mantle Setting, Diamonds and Diamond Exploration. Geological Society of Australia Special Publication No 14, vol. 2, 966–989.

Jaques, A. L., Hall, A. E., Sheraton, J., Smith, C. B., & Roksandic, Z. (1994). Peridotitic planar octahedral diamonds from the Ellendale lamproite pipes, Western Australia. In Diamonds: Characterization, Genesis and Exploration. Proceedings of the Fifth International Kimberlite Conference. CPRM, Rio de Janeiro, Brazil, Vol. 2, 69-77.

Javoy, M., Pineau, F., & Delorme, H. (1986). Carbon and nitrogen isotopes in the mantle. Chemical geology, 57(1-2), 41-62.

Kasting J.F., Eggler D.H., Raeburn S.P. (1993). Mantle redox evolution and the oxidation state of the archean atmosphere. Journal of Geology, 101, 245–57.

Keleman, P.B. and Manning, C.E. (2015). Reevaluating carbon fluxes in subduction zones, what goes down, mostly comes up. Proceedings of the National Academy of Sciences, 112, E3997-4006

Kirkley, M. B., Gurney, J. J., Otter, M. L., Hill, S. J., & Daniels, L. R. (1991). The application of C isotope measurements to the identification of the sources of C in diamonds: a review. Applied Geochemistry, 6(5), 477-494.

Li Z.X.A. and Lee C.T.A. (2004) The constancy of upper mantle fO2 through time inferred from V/Sc ratios in basalts. Earth and Planetary Science Letters, 228(3–4), 483–493.

Li, K., Li, L., Pearson, D. G., & Stachel, T. (2019). Diamond isotope compositions indicate altered igneous oceanic crust dominates deep carbon recycling. Earth and Planetary Science Letters, 516, 190-201.

Luth, R.W. & Stachel, T. (2014). The buffering capacity of lithospheric mantle: implications for diamond formation. Contributions to Mineralogy and Petrology, 168, 1083.

McCammon, C. (2005). The paradox of mantle redox. Science, 308 (5723), 807-808.

Mikhail, S., Guillermier, C., Franchi, I.A., Beard, A.D., Crispin, K., Verchovsky, A.B., Jones, A.P. & Milledge, H.J. (2014). Empirical evidence for the fractionation of carbon isotopes between diamond and iron carbide from the Earth's mantle. Geochemistry, Geophysics, Geosystems, 15 (4), 855-866.

Mikhail, S., Verchovsky, A. B., Howell, D., Hutchison, M. T., Southworth, R., Thomson, A. R., Warburton, P., Jones, A.P. and Milledge, H. J. (2014). Constraining the internal variability of the stable isotopes of carbon and nitrogen within mantle diamonds. *Chemical Geology*, *366*, 14-23.

Milledge, H. J., Mendelssohn, M. J., Seal, M., Rouse, J. E., Swart, P. K., & Pillinger, C. T. (1983). Carbon isotopic variation in spectral type II diamonds. Nature, 303(5920), 791.

Nestola, F., Jung, H., & Taylor, L. A. (2017). Mineral inclusions in diamonds may be synchronous but not syngenetic. Nature communications, 8, 14168.

Nestola, F., Jacob, D.E., Pamato, M.G., Pasqualetto, L., Oliveira, B., Greene, S., Perritt, S., Chinn, I., Milani, S., Kueter, N. & Sgreva, N. (2019). Protogenetic garnet inclusions and the age of diamonds. Geology 47, 431-434.

Nicklas, R. W., Puchtel, I. S., & Ash, R. D. (2018). Redox state of the Archean mantle: Evidence from V partitioning in 3.5–2.4 Ga komatiites. Geochimica et Cosmochimica Acta, 222, 447-466.

Nicklas, R.W., Puchtel, I.S., Ash, R.D., Piccoli, P.M., Hanski, E., Nisbet, E.G., Waterton, P., Pearson, D.G. & Anbar, A.D. (2019). Secular mantle oxidation across the Archean-Proterozoic boundary: Evidence from V partitioning in komatiites and picrites. Geochimica et Cosmochimica Acta, 250, pp.49-75.

Palot, M., Pearson, D.G., Stern, R.A., Stachel, T., & Harris, J.W. (2013). Multiple growth events, processes and fluid sources involved in diamond genesis: a micro-analytical study of sulphide-bearing diamonds from Finsch mine, RSA. Geochimica et Cosmochimica Acta, 106, 51-70.

Pearson, D.G., Shirey, S.B., Harris, J.W., & Carlson, R.W. (1998). Sulphide inclusions in diamonds from the Koffiefontein kimberlite, S Africa: constraints on diamond ages and mantle Re–Os systematics. Earth and Planetary Science Letters, 160(3-4), 311-326.

Petts, D.C., Chacko, T., Stachel, T., Stern, R.A., & Heaman, L.M. (2015). A nitrogen isotope fractionation factor between diamond and its parental fluid derived from detailed SIMS analysis of a gem diamond and theoretical calculations. Chemical Geology, 410, 188-200.

Reutsky, V.N., Borzdov, Y.M., & Palyanov, Y.N. (2012). Effect of diamond growth rate on carbon isotope fractionation in Fe–Ni–C system. Diamond and related materials, 21, 7-10.

Reutsky, V.N., Palyanov, Y.N., Borzdov, Y.M., & Sokol, A.G. (2015). Isotope fractionation of carbon during diamond crystallization in model systems. Russian Geology and Geophysics, 56(1-2), 239-244.

Richardson, S.H. (1986). Latter-day origin of diamonds of eclogitic paragenesis. Nature, 322(6080), 623.

Richardson, S.H. and Harris, J.W. (1997). Antiquity of peridotitic diamonds from the Siberian craton. Earth and Planetary Science Letters, 151(3-4), 271-277.

Richardson, S.H., Erlank, A.J., Harris, J.W., & Hart, S.R. (1990). Eclogitic diamonds of Proterozoic age from Cretaceous kimberlites. Nature, 346(6279), 54.

Richardson, S.H., Gurney, J.J., Erlank, A.J., & Harris, J.W. (1984). Origin of diamonds in old enriched mantle. Nature, 310(5974), 198.

Richardson, S.H., Pöml, P.F., Shirey, S.B., & Harris, J.W. (2009). Age and origin of peridotitic diamonds from Venetia, Limpopo Belt, Kaapvaal–Zimbabwe craton. Lithos, 112, 785-792.

Richardson, S.H., Shirey, S.B., & Harris, J.W. (2004). Episodic diamond genesis at Jwaneng, Botswana, and implications for Kaapvaal craton evolution. Lithos, 77(1-4), 143-154.

Richardson, S.H., Shirey, S.B., Harris, J.W., & Carlson, R.W. (2001). Archean subduction recorded by Re–Os isotopes in eclogitic sulfide inclusions in Kimberley diamonds. Earth and Planetary Science Letters, 191(3-4), 257-266.

Rollinson H., Adetunji, J., Lenaz, D., & Szilas, K. (2017) Archaean chromitites show constant Fe3 +/ΣFe in Earth's asthenospheric mantle since 3.8 Ga. Lithos 282–283:316-325.

Satish-Kumar, M., So, H., Yoshino, T., Kato, M., & Hiroi, Y. (2011). Experimental determination of carbon isotope fractionation between iron carbide melt and carbon: 12C-enriched carbon in the Earth's core? Earth and Planetary Science Letters, 310 (3-4), 340-348.

Schulze, D.J., Harte, B., Page, F.Z., Valley, J.W., Channer, D.M.DeR., and Jaques, A.L., 2013, Anticorrelation between low δ13C of eclogitic diamonds and high δ18O of their coesite and garnet inclusions requires a subduction origin: Geology, v. 41, p. 455–458.

Schrauder, M. and Navon, O. (1993). Solid carbon dioxide in a natural diamond. Nature, 365 (6441), 42.

Shields, G. and Veizer, J. (2002). Precambrian marine carbonate isotope database: Version 1.1. *Geochemistry, Geophysics, Geosystems*, *3* (6), 1-12.

Shilobreeva, S., Martinez, I., Busigny, V., Agrinier, P., & Laverne, C. (2011). Insights into C and H storage in the altered oceanic crust: Results from ODP/IODP Hole 1256D. Geochimica et Cosmochimica Acta, 75(9), 2237-2255.

Shirey, S.B. and Richardson, S.H. (2011). Start of the Wilson cycle at 3 Ga shown by diamonds from subcontinental mantle. Science, 333(6041), 434-436.

Shirey, S.B., Richardson, S.H., & Harris, J.W. (2009). Mesoarchean to Mesoproterozoic Re-Os ages for sulfide inclusions in Orapa diamonds and implications for Kaapvaal-Zimbabwe craton development. In 9th International Kimberlite Conference Extended Abstract No. 9IKC-A-00365

Shu, Q., Brey, G.P., Hoefer, H.E., Zhao, Z., & Pearson, D.G. (2016). Kyanite/corundum eclogites from the Kaapvaal Craton: subducted troctolites and layered gabbros from the Mid-to Early Archean. Contributions to Mineralogy and Petrology, 171(2), 11.

Smart, K.A., Chacko, T., Stachel, T., Muehlenbachs, K., Stern, R.A., & Heaman, L.M. (2011). Diamond growth from oxidized carbon sources beneath the Northern Slave Craton, Canada: a δ13C–N study of eclogite-hosted diamonds from the Jericho kimberlite. Geochimica et Cosmochimica Acta, 75(20), 6027-6047.

Smit, K.V., Shirey, S.B., Hauri, E.H., & Stern, R.A. (2019b). Sulfur isotopes in diamonds reveal differences in continent construction. Science, 364(6438), 383-385.

Smit, K.V., Shirey, S.B., Richardson, S.H., le Roex, A.P., & Gurney, J.J. (2010). Re–Os isotopic composition of peridotitic sulphide inclusions in diamonds from Ellendale, Australia: Age constraints on Kimberley cratonic lithosphere. Geochimica et Cosmochimica Acta, 74(11), 3292-3306.

Smit, K.V., Shirey, S.B., Stern, R.A., Steele, A., & Wang, W. (2016). Diamond growth from C–H–N–O recycled fluids in the lithosphere: Evidence from CH4 micro-inclusions and δ13C–δ15N–N content in Marange mixed-habit diamonds. Lithos, 265, 68-81.

Smit, K.V., Stachel, T., Luth, R.W., & Stern, R.A. (2019a). Evaluating mechanisms for eclogitic diamond growth: An example from Zimmi Neoproterozoic diamonds (West African craton). Chemical Geology, 520, 21-32.

Smit, K.V., Stachel, T., & Stern, R.A. (2014). Diamonds in the Attawapiskat area of the Superior craton (Canada): evidence for a major diamond-forming event younger than 1.1 Ga. Contributions to Mineralogy and Petrology, 167(1), 962.

Smith, E.M., Shirey, S.B., Nestola, F., Bullock, E.S., Wang, J., Richardson, S.H., & Wang, W. (2016). Large gem diamonds from metallic liquid in Earth's deep mantle. Science, 354(6318), 1403-1405.

Sobolev, V.S. and Sobolev, N.V., 1980, New proof of very deep subsidence of eclogitized crustal rocks: Doklady Akadamiya Nauk SSSR, v. 250, 683-685 (in Russian).

Stachel, T. and Harris, J.W. (2009). Formation of diamond in the Earth's mantle. Journal of Physics: Condensed Matter, 21, 364206.

Stachel, T. and Luth, R.W. (2015). Diamond formation – where, when and how? Lithos, 220-223, 200-220.

Stachel, T., Banas, A., Aulbach, S., Smit, K.V., Wescott, P., Chinn, I., Fisher, D., & Kong, J. (2017b). The Victor diamond mine (Superior craton, Canada) – a new paradigm for exploration in unconventional settings. International Kimberlite Conference: Extended Abstracts, 11.

Stachel, T., Banas, A., Muehlenbachs, K., Kurszlaukis, S., & Walker, E.C. (2006). Archean diamonds from Wawa (Canada): samples from deep cratonic roots predating cratonization of the Superior Province. Contributions to Mineralogy and Petrology, 151(6), 737.

Stachel, T., Chacko, T., & Luth, R.W. (2017a). Carbon isotope fractionation during diamond growth in depleted peridotite: Counterintuitive insights from modelling water-maximum CHO fluids as multi-component systems. Earth and Planetary Science Letters, 473, 44-51.

Stachel, T., Harris, J. W., & Muehlenbachs, K. (2009). Sources of carbon in inclusion bearing diamonds. Lithos, 112, 625-637.
Stachel, T., Harris, J.W., Hunt, L., Muehlenbachs, K., Kobussen, A.F., and Edinburgh Ion Micro-Probe Facility, (2018). Argyle diamonds: How sub- duction along the Kimberley craton edge generated the world's biggest diamond deposit: Society of Economic Geologists, Special Publication 20, 145–167.
Stern, R.A., Palot, M., Howell, D., Stachel, T., Pearson, D.G., Cartigny, P., & Oh, A. (2014). Methods and reference materials for SIMS diamond C-and N-isotope analysis. Canadian Centre for Isotopic Microanalysis. Research Report 14-01. University of Alberta, Education and Research Archive. http://hdl. handle. net/10402/era. 38738.
Sunagawa, I. (1990) Growth and morphology of diamond crystals under stable and metastable conditions. Journal of Crystal Growth, 99(1–4), 1156.
Sverjensky D.A. and Huang F. (2015) Diamond formation due to a pH drop during fluid-rock interactions. Nat. Commun. 6.
Tappert, R., Stachel, T., Harris, J.W., Muehlenbachs, K., Ludwig, T., & Brey, G. P. (2005). Subducting oceanic crust: The source of deep diamonds. Geology, 33(7), 565-568.
Thomassot, E., Cartigny, P., Harris, J.W., & Viljoen, K.F. (2007). Methane-related diamond crystallization in the Earth's mantle: stable isotope evidences from a single diamond-bearing xenolith. Earth and Planetary Science Letters, 257(3-4), 362-371.
Thomassot, E., Cartigny, P., Harris, J.W., Lorand, J.P., Rollion-Bard, C., & Chaussidon, M. (2009). Metasomatic diamond growth: A multi-isotope study (13C, 15N, 33S, 34S) of sulphide inclusions and their host diamonds from Jwaneng (Botswana). Earth and Planetary Science Letters, 282(1-4), 79-90.
Timmerman, S., Koornneef, J.M., Chinn, I.L., & Davies, G.R. (2017). Dated eclogitic diamond growth zones reveal variable recycling of crustal carbon through time. Earth and Planetary Science Letters, 463, 178-188.
Timmerman, S., Krebs, M.Y., Pearson, D.G., & Honda, M. (2019a). Diamond-forming media through time–Trace element and noble gas systematics of diamonds formed over 3 billion years of Earth's history. Geochimica et Cosmochimica Acta, 257, 266-283.
Timmerman, S., Honda, H., Zhang, X., Jaques, A.L., Bulanova, G., Smith. C.B., & Burnham, A.D.S., (2019b). Contrasting noble gas compositions of peridotitic and eclogitic monocrystalline diamonds from the Argyle lamproite, Western Australia. Lithos, 344-345, 193-206.
Tiraboschi, C., Tumiati, S., Sverjensky, D., Pettke, T., Ulmer, P., & Poli, S. (2018). Experimental determination of magnesia and silica solubilities in graphite-saturated and redox-buffered high-pressure COH fluids in equilibrium with forsterite+ enstatite and magnesite + enstatite. Contributions to Mineralogy and Petrology, 173(1), 2.
Trail D., Watson E.B. and Tailby N. D. (2011) The oxidation state of Hadean magmas and implications for early Earth's atmosphere. Nature, 480(7375), 79–82.
Walter, M.J., Kohn, S.C., Araujo, D., Bulanova, G.P., Smith, C.B., Gaillou, E., Wang, J., Steele, A. and Shirey, S.B., 2011. Deep mantle cycling of oceanic crust: evidence from diamonds and their mineral inclusions. Science, 334(6052), 54-57.
Wang, A., Pasteris, J.D., Meyer, H.O., & Dele-Duboi, M.L. (1996). Magnesite-bearing inclusion assemblage in natural diamond. Earth and Planetary Science Letters, 141(1-4), 293-306.
Weiss, Y., Kessel, R., Griffin, W.L., Kiflawi, I., Klein-BenDavid, O., Bell, D.R., Harris, J.W., & Navon, O. (2009). A new model for the evolution of diamond-forming fluids: Evidence from microinclusion-bearing diamonds from Kankan, Guinea. Lithos, 112, 660-674.
Welbourn, C.M., Rooney, M.L.T., & Evans, D.J.F. (1989). A study of diamonds of cube and cube-related shape from Jwaneng mine. Journal of Crystal Growth, 94, 229-252.
Woodland A.B., Kornprobst J., Tabit A., (2006). Ferric iron in orogenic lherzolite massifs and controls of oxygen fugacity in the upper mantle. Lithos, 89, 222–41
Zedgenizov, D.A. and Harte, B. (2004). Microscale variations of δ13C and N content within a natural diamond with mixed-habit growth. Chemical Geology, 205(1-2), 169-175.
Zedgenizov, D.A. Harte, B. EIMF, Shatsky, V.S., Politov, A.A., Rylov, G.M., & Sobolev, N.V. (2006). Directional chemical variations in diamonds showing octahedral growth following cuboid growth. Contributions to Mineralogy and Petrology, 151, 45-57.

Figure Captions

Figure 1: Illustration showing the occurrence of diamond growth events throughout Earth's history. The deposits are grouped based upon their location; Australia (left), Canada, Russia, and Africa (right). White symbols represent deposits studied in this paper. Square symbols represent peridotitic diamond growth events (Hz and Lh denote harzburgitic and lherzolitic classifications where reported), while diamond symbols represent eclogitic diamond growth events. Fibrous diamond growth events (circle symbols) noted here reflect the kimberlite eruption age. A table containing all of the dates and references are provided in the Supplementary Material (Table S1).

Figure 2: Histograms for all of the analyses of peridotitic (right-hand side) and eclogitic (left-hand side) diamonds studied here. Where available, published literature data (combustion data only, provided in Table S3) are shown in grey. The representation of the two datasets is not additive (one on top of the other) but one is set in front of the other. Note that the scales on the y-axis vary between plots. The histograms use 0.5 ‰ binning.

Figure 3: Cathodoluminescence images of a selection of samples showing varied growth histories. (A) JWR 8; Jwaneng, (B) ORS 2; Orapa, (C) DP-4; De Beers Pool, (D) DDMI 199; Diavik, (E) JWR 18; Jwaneng. All scale bars are 200 μm long.

Figure 4: Histograms showing the data obtained from all of the samples, compared to those where only diamonds whose CL indicates single growth event are counted, separated based upon inclusion type.

Figure 5: Theoretical fractionation plots for diamond growth from a fluid with a starting $\delta^{13}C$ value of -5 ‰ (yellow star; f_c represents the remaining fraction of carbon-bearing species in the diamond-forming fluid). The offset between the initial diamond growth and the fluid is governed by the carbon species in the fluid. The plots show diamond growth from (a) a CO_2 (oxidized) fluid, (b) a CO_3 (oxidized) fluid, and (c) a CH_4 (reduced) fluid. Plot (d) shows a more complex multicomponent system, with the fluid containing both oxidized and reduced species (namely CO_2 and CH_4) in varying proportions (10 mol% CO_2 - blue, 50 % - black, 89 % - red lines). Note that in these multicomponent calculations, the diamond's $\delta^{13}C$ values always trend to less negative values irrespective of the dominant carbon species. Plot (d) after Stachel et al. (2017a).

Figure 6: CL images of (A) DBP-363_5, (B) V-336, (C) DBP-9, (D) DBP-460_9, with their SIMS $\delta^{13}C$ analysis locations marked and red arrows showing growth direction. The graphs show the $\delta^{13}C$ values plotted against N concentration. The lines connect the analyses in order, arrows showing the growth direction.

Figure 7: Box and Whisker plot showing the $\delta^{13}C$ data from this study (bold colours), as well as data from the literature (combustion plus SIMS data; faint colours), in a

chronological order. Where single outliers are more than 3 ‰ from the remaining data, they have been marked as single data points (in Panda, Diavik and Venetia). The literature data plotted here is provided in Table 3 (with the total dataset, including references, provided in Table S3).

Figure 8: MDS and PCA plots for peridotitic diamonds. (a) MDS plot showing only $\delta^{13}C$ data. Note how the Wawa data (red diamonds) do not overlap with the older Diavik (black circles) and De Beers Pool (black squares) data. (b) PCA plot of $\delta^{13}C$ - N data. Given that MDS is a transformation that assigns input information a unitless (arbitrary unit) value (as it preserves only the relationships between data rather than specific information), we have not placed a scale on either axis of the MDS plot.

Figure 9: MDS and PCA plots for eclogitic diamonds. (a) MDS plot showing only $\delta^{13}C$ data. (b) PCA plot of $\delta^{13}C$ -N data. The dashed line represents a contour which contains 71% of all the data. Note how the Argyle data falls almost exclusively outside of this cluster. (c) PCA plot showing $\delta^{13}C$ - N data from only the Orapa samples.

Table 1: Details of the diamond samples

Information regarding the source locations and quantities of the diamonds studied in this paper. References provided are the original works that dated the inclusions. In cases where two references are provided, the second notes the study where the diamonds have been sourced from which is separate to the original dating study.

Table 2: Summary of the $\delta^{13}C$ and N data

The statistics generated from the $\delta^{13}C$ and N datasets for both peridotitic and eclogitic diamonds in this study. The Δ symbol represents the 'variation per sample'. The 'Pear Skew' value is the Pearson Coefficient of Skewness which is calculated as [3 x (average – median)] / standard deviation. The "average of samples' averages / medians" rows of data have been obtained by taking either the average or median values from each sample individually, and then taking an average of them per deposit. This was done to see if over analysis of an individual diamond was affecting the distribution of the data as a whole. The final rows show the differences between the

data as a whole and of the individual stones. The average of these differences are ~0.1 ‰ for the P-type data, and ~0.2 ‰ for the E-type data. Only the Orapa 3 Ga and 2.1 Ga samples exceed differences of 0.25 ‰, showing that overall individual samples have not been over-analysed in this study.

Table 3: Summary of single growth vs multiple growth data

The statistics of the total P-type and E-type $\delta^{13}C$ and N datasets compared against the reduced datasets obtained from samples that exhibit only a single growth event (as interpreted from their CL imagery).

Table 4: Literature $\delta^{13}C$ data

Table showing the statistics of the literature data presented in Figure 7. *n* represents the number of diamonds, with each diamond providing a single data point. * Three locations utilize SIMS data where the first number is the number of diamonds, while the subsequent number in brackets represents the total number of analyses. The total dataset summarized here is provided in Table S3, including all relevant references.

SUPPLEMENTARY MATERIAL:

Table S1) References for Figure 1.

This table contains all of the references used to make Figure 1, showing all of the documented diamond growth events in Africa, Russia, Canada and Australia.

Table S2) Total $\delta^{13}C$ and N data from this study

This table contains all of the $\delta^{13}C$ and N data obtained in this study, with the diamond samples separated based upon their inclusion paragenesis.

Table S3) Literature $\delta^{13}C$ data

This table contains all of the literature data, referenced in the paper and its figures, along with the references from which the data were obtained.

Supplementary Material 1: Detailed methodology used for the multi-dimensional scaling (MDS) and principal component analysis (PCA) presented in this study.

Supplementary Material 2: Reference list for Table S1 and S3.

Table 1

Location	Craton	Paragenesis	Number of samples	Age
Argyle	Kimberley	Eclogitic	10	1.58 Ga
De Beers Pool	Kaapvaal	Eclogitic	8	2.9 Ga
De Beers Pool	Kaapvaal	Peridotitic	21	3.2 Ga
Diavik	Slave	Eclogitic	9	1.86 Ga
Diavik	Slave	Peridotitic	9	~ 3.3 Ga
Ellendale	Kimberley	Peridotitic	13	1.4 Ga
Jwaneng	Kaapvaal	Eclogitic	16	1.0 / 2.1 / 3.0 Ga
Orapa	Kaapvaal	Eclogitic	13	1.0 / 2.1 / 3.0 Ga
Udachnaya	Siberian	Peridotitic	15	2.0 Ga
Venetia	Limpopo Belt	Peridotitic	19	< 2.3 Ga
Wawa	Superior	Peridotitic	11	> 2.7 Ga

Table 2

	Orapa 3 Ga		Jwaneng 3 Ga		De Beers P
	δ13C (VPDB)	[N] at. ppm	δ13C (VPDB)	[N] at. ppm	δ13C (VPDB)
No. of samples	6	6	6	6	8
No. of analyses	51	51	52	52	51
average	-6.10	596	-5.96	747	-5.61
min	-9.24	8	-17.09	1	-6.84
max	-4.38	1249	-2.98	2661	-3.30
average Δ	0.86	701	3.71	937	1.42
min Δ	0.28	318	0.43	231	0.53
max Δ	1.34	1166	12.13	2516	2.55
Q1	-7.70	171	-5.37	397	-6.11
Q3	-4.92	920	-4.83	1060	-5.27
median	-5.35	748	-5.13	891	-5.64
st dev	1.55	397	3.10	519	0.71
Pear Skew	-1.45	-1.15	-0.80	-5.15	0.15
Average of samples'					
averages	-6.83	406	-6.18	714	-5.52
medians	-6.84	408	-6.52	606	-5.44
Difference between					
averages	0.73	190	0.23	33	-0.09
medians	1.49	340	1.39	285	-0.20

	Diavik ~3.3 Ga		De Beers Pool 3.2 Ga		Wawa :
	δ13C (VPDB)	[N] at. ppm	δ13C (VPDB)	[N] at. ppm	δ13C (VPDB)
No. of samples	9	9	21	21	11
No. of analyses	56	57	135	135	65
average	-5.12	132	-5.45	76	-3.58
min	-6.29	0	-8.39	2	-4.48
max	-4.19	1131	-2.87	1477	-1.87
average Δ	0.55	334	1.20	230	0.35
min Δ	0.18	46	0.19	4	0.08
max Δ	1.47	1124	2.51	1463	0.95
Q1	-5.39	11	-5.72	10	-4.16
Q3	-4.52	120	-4.98	45	-2.96
median	-5.27	44	-5.26	20	-3.76
st dev	0.55	236	0.84	195	0.72
Pear Skew	0.81	-0.56	-0.66	0.86	0.75
Average of samples'					
averages	-5.04	131	-5.47	5	-3.35
medians	-5.05	80	-5.45	28	-3.36
Difference between					
averages	-0.08	0	0.03	71	-0.23

Table 3

	TOTAL P-TYPE DATA		SINGLE GROWTH P-TYPE		TOTAL E-T
	δ13C (VPDB)	[N] at. ppm	δ13C (VPDB)	[N] at. ppm	δ13C (VPDB)
No. of samples	88	88	45	45	56
No. of analyses	504	506	244	245	404
average	-4.79	221	-4.73	171	-6.74
min	-8.39	0	-8.39	2	-17.09
max	-1.87	3073	-1.87	1275	-2.07
average Δ	0.85	369	0.49	147	1.53
min Δ	0.07	4	0.07	4	0.10
max Δ	2.80	3066	2.56	1013	12.13
Q1	-5.42	19	-5.38	21	-7.90
Q3	-4.07	222	-4.02	204	-5.09
median	-4.87	52	-4.76	45	-5.65
st dev	1.12	369	1.16	263	2.48
Pear Skew	0.23	1.37	0.08	1.44	-1.32

Table 4

Location	PANDA	DIAVIK	FINSCH	DE BEERS POOL	DE BEERS POOL
Age (Ga)	3.52	3.5-3.3	3.3-3.3	3.3-3.2	2.9
Paragenesis	P-TYPE	P-TYPE	P-TYPE	P-TYPE	E-TYPE
n=	129	110	70	213	53
min	-14.05	-11.50	-8.57	-6.98	-15.97
Q1	-5.45	-5.44	-6.59	-5.42	-5.62
median	-5.12	-5.13	-6.12	-5.18	-5.13
Q3	-4.86	-4.62	-5.64	-4.84	-4.59
max	-2.98	-2.10	-2.62	-0.93	-3.06

Figure 1

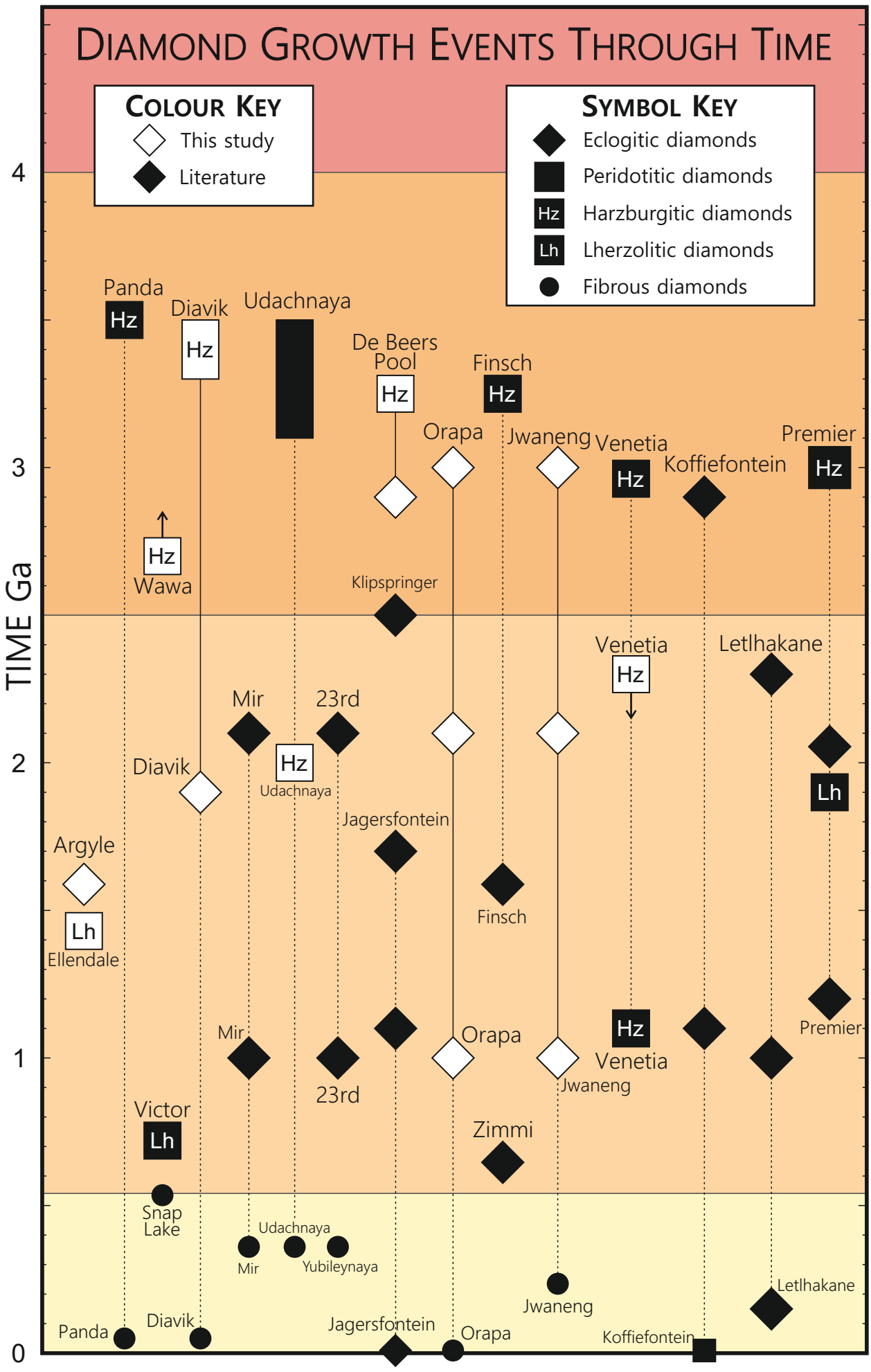
DIAMOND GROWTH EVENTS THROUGH TIME
COLOUR KEY
This study
Literature
SYMBOL KEY
Eclogitic diamonds
Peridotitic diamonds
Hz Harzburgitic diamonds
Lh Lherzolitic diamonds
Fibrous diamonds
TIME Ga
4
3
2
1
0
Panda
Hz
Diavik
Hz
Udachnaya
De Beers Pool
Hz
Finsch
Hz
Orapa
Jwaneng
Venetia
Hz
Koffiefontein
Premier
Hz
Hz
Wawa
Klipspringer
Venetia
Hz
Letlhakane
Mir
23rd
Diavik
Hz
Udachnaya
Lh
Jagersfontein
Argyle
Lh
Ellendale
Finsch
Mir
Hz
Venetia
Premier
Orapa
23rd
Jwaneng
Victor
Lh
Zimmi
Snap Lake
Udachnaya
Mir
Yubileynaya
Jwaneng
Letlhakane
Panda
Diavik
Jagersfontein
Orapa
Koffiefontein

Figure 2

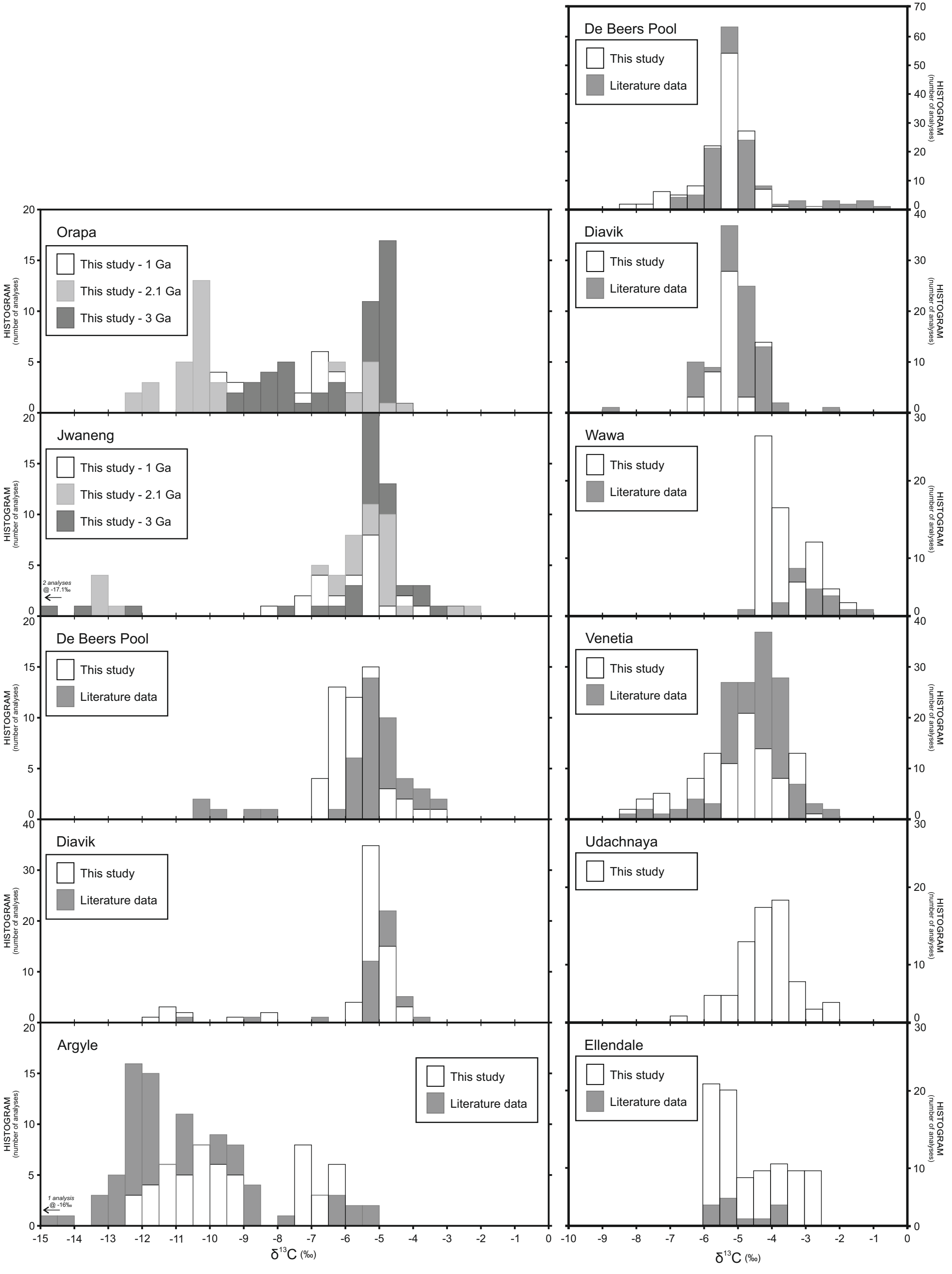
De Beers Pool
This study
Literature data
Orapa
This study - 1 Ga
This study - 2.1 Ga
This study - 3 Ga
Diavik
This study
Literature data
Jwaneng
This study - 1 Ga
This study - 2.1 Ga
This study - 3 Ga
2 analyses
@ -17.1‰
Wawa
This study
Literature data
De Beers Pool
This study
Literature data
Venetia
This study
Literature data
Diavik
This study
Literature data
Udachnaya
This study
Argyle
This study
Literature data
1 analysis
@ -16‰
Ellendale
This study
Literature data
HISTOGRAM
(number of analyses)
δ13C (‰)

Figure 3

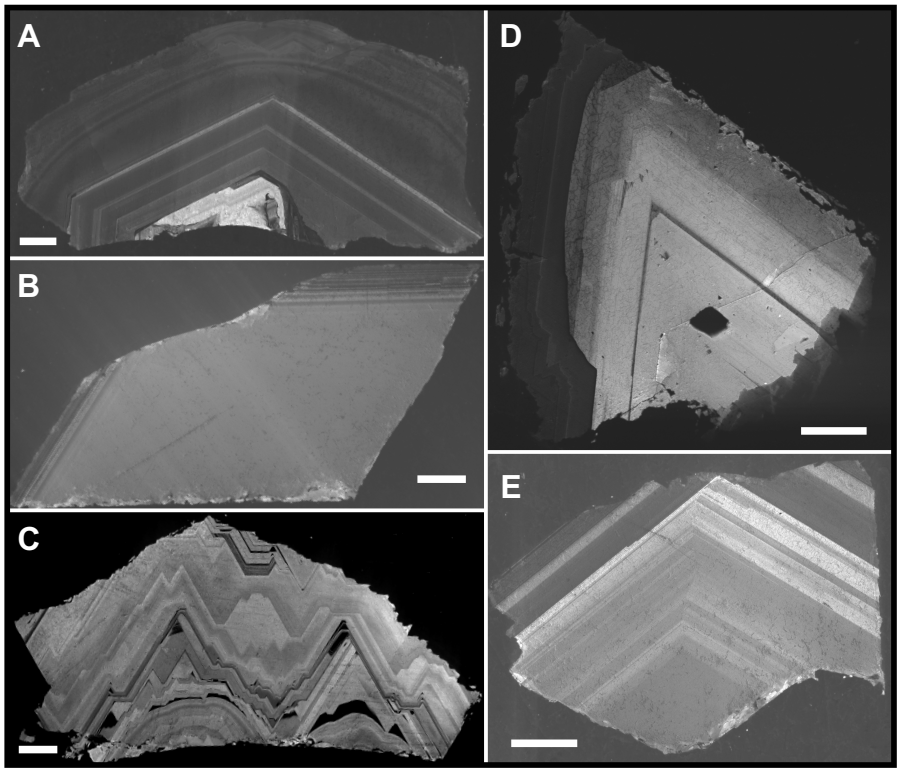

Figure 4

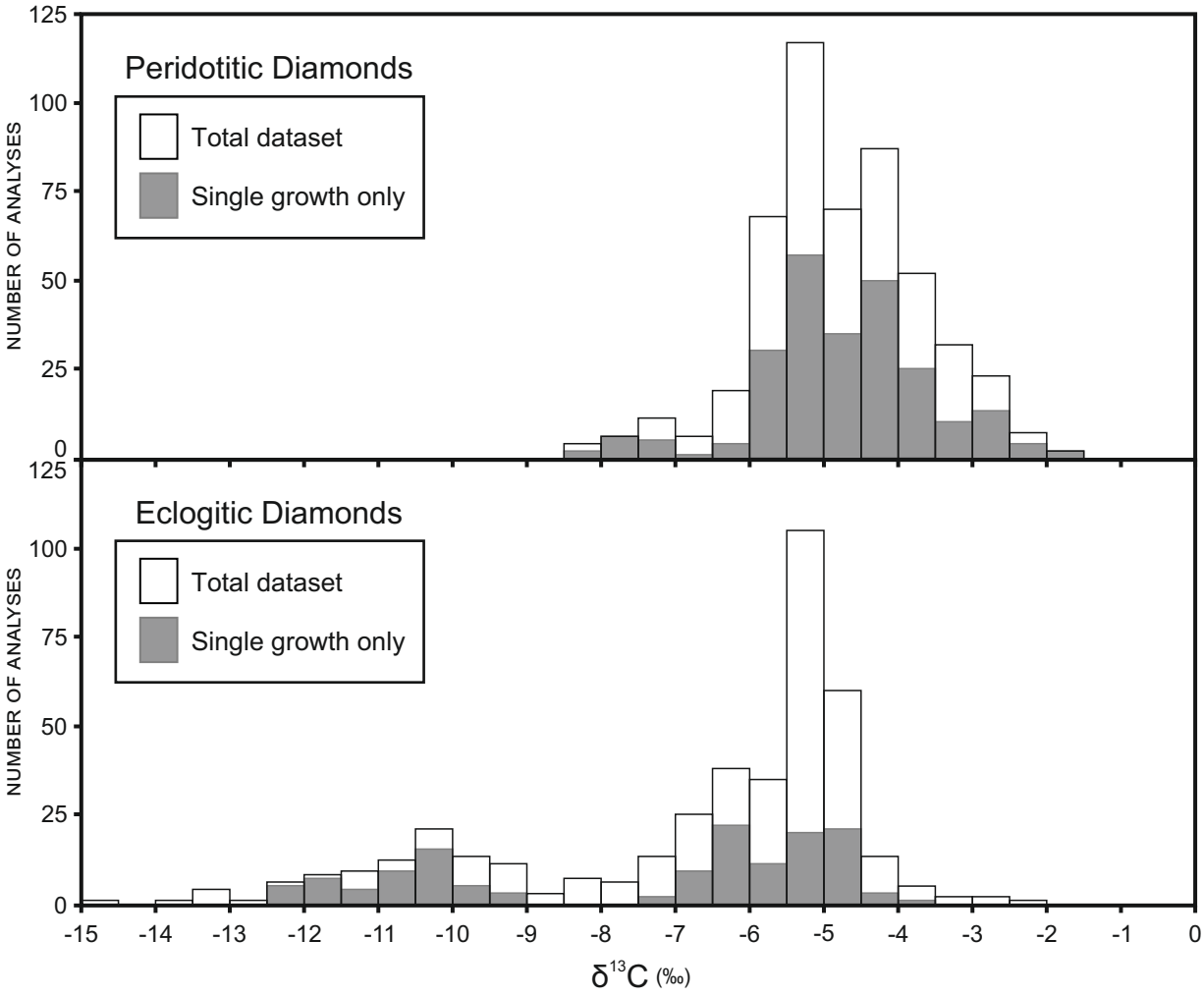
Peridotitic Diamonds
Total dataset
Single growth only
NUMBER OF ANALYSES
125
100
75
50
25
0
Eclogitic Diamonds
Total dataset
Single growth only
NUMBER OF ANALYSES
125
100
75
50
25
0
-15
-14
-13
-12
-11
-10
-9
-8
-7
-6
-5
-4
-3
-2
-1
0
δ13C (‰)

Figure 5

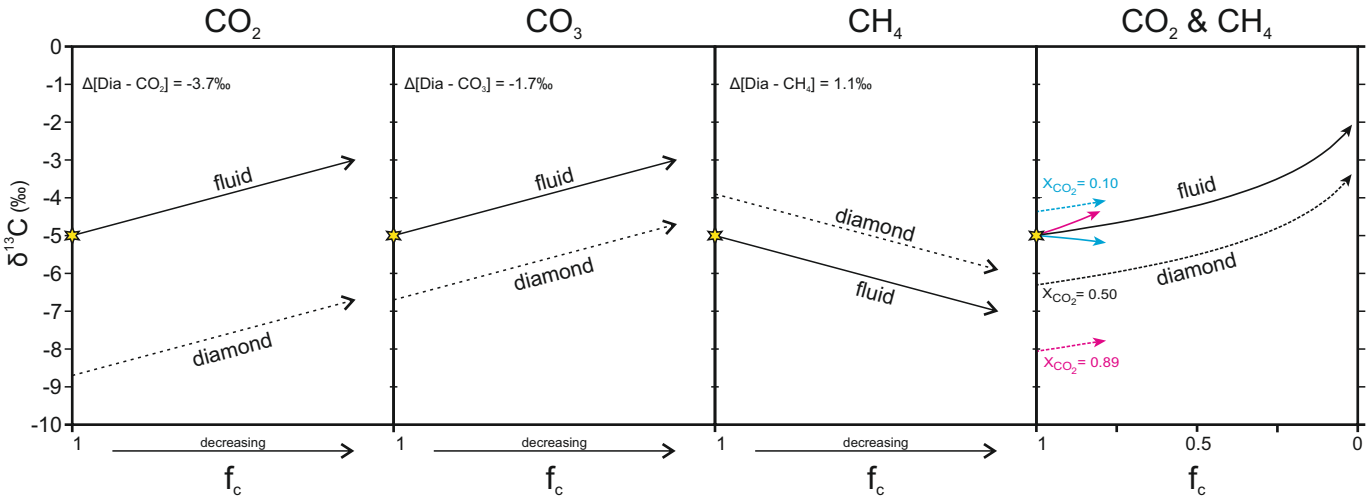
CO2
CO3
CH4
CO2 & CH4
Δ[Dia - CO2] = -3.7‰
Δ[Dia - CO3] = -1.7‰
Δ[Dia - CH4] = 1.1‰
fluid
diamond
δ13C (‰)
0
-1
-2
-3
-4
-5
-6
-7
-8
-9
-10
1
decreasing
fc
0.5
0
XCO2= 0.10
XCO2= 0.50
XCO2= 0.89

Figure 6

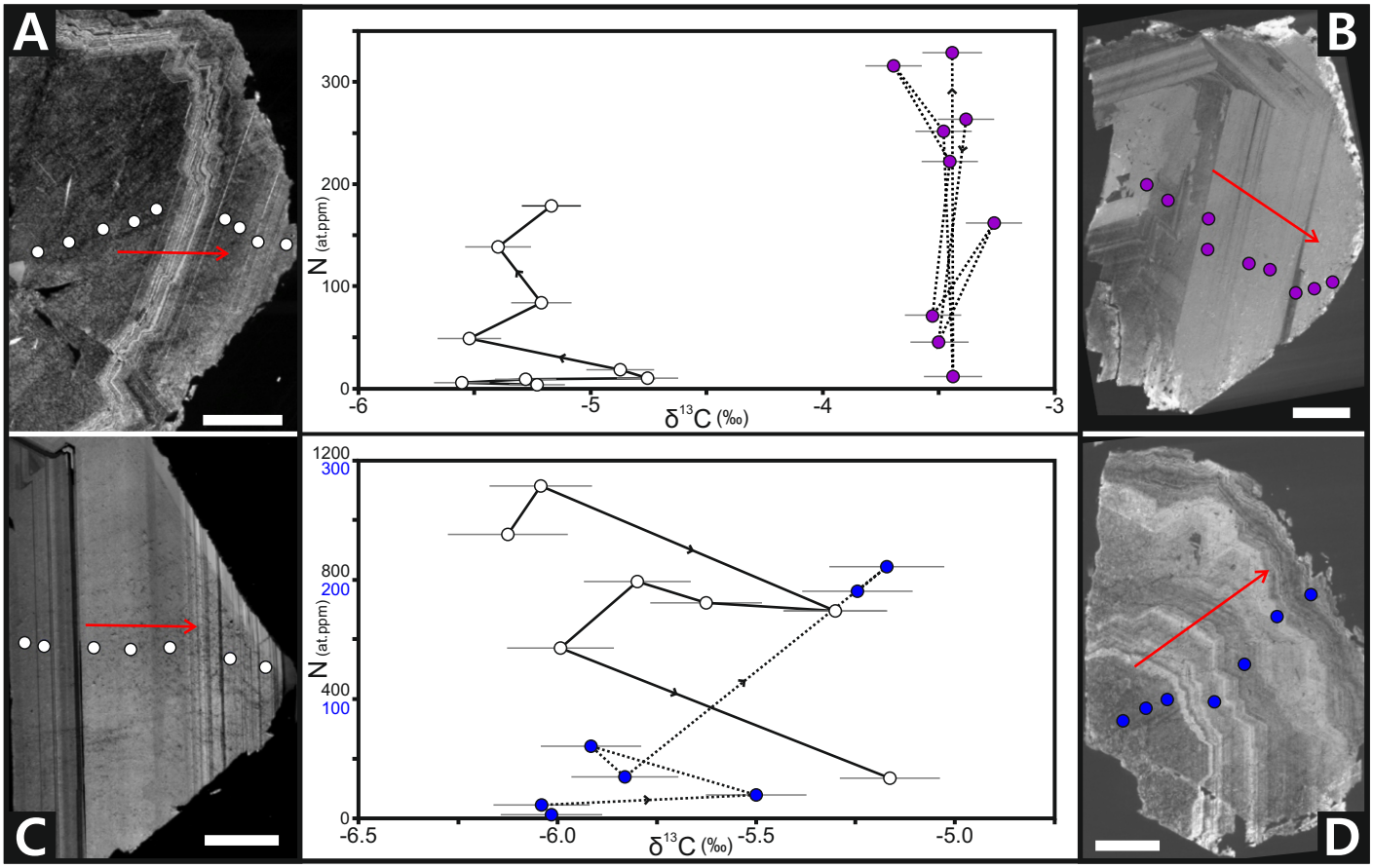
A
B
C
D
N (at.ppm)
300
200
100
0
-6
-5
-4
-3
δ13C (‰)
1200
300
800
200
400
100
0
-6.5
-6.0
-5.5
-5.0
δ13C (‰)

Figure 7

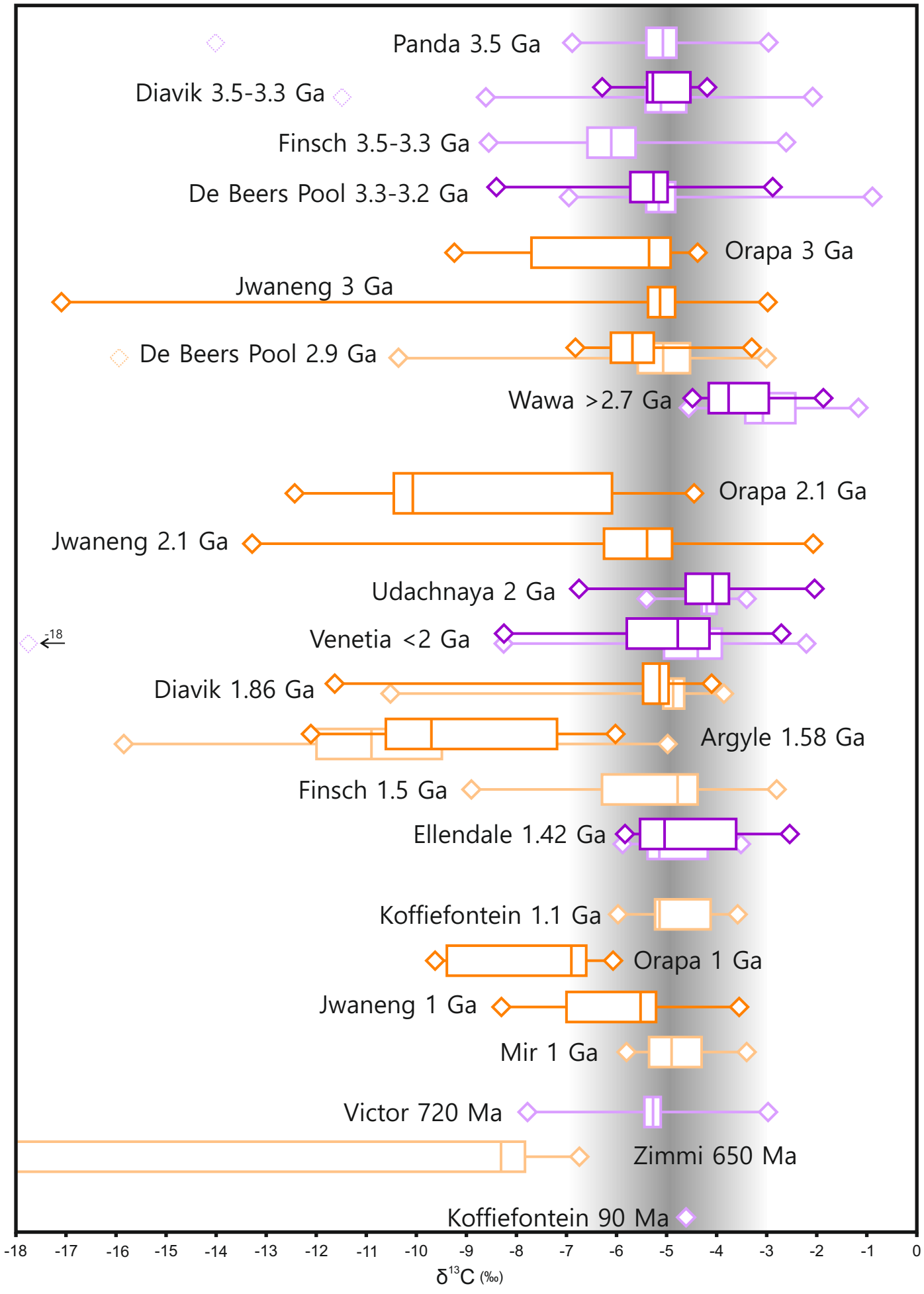
Panda 3.5 Ga
Diavik 3.5-3.3 Ga
Finsch 3.5-3.3 Ga
De Beers Pool 3.3-3.2 Ga
Orapa 3 Ga
Jwaneng 3 Ga
De Beers Pool 2.9 Ga
Wawa >2.7 Ga
Orapa 2.1 Ga
Jwaneng 2.1 Ga
Udachnaya 2 Ga
Venetia <2 Ga
Diavik 1.86 Ga
Argyle 1.58 Ga
Finsch 1.5 Ga
Ellendale 1.42 Ga
Koffiefontein 1.1 Ga
Orapa 1 Ga
Jwaneng 1 Ga
Mir 1 Ga
Victor 720 Ma
Zimmi 650 Ma
Koffiefontein 90 Ma
-18 -17 -16 -15 -14 -13 -12 -11 -10 -9 -8 -7 -6 -5 -4 -3 -2 -1 0
δ13C (‰)
Eclogitic data - This Study
Peridotitic data - This Study
Eclogitic data - Literature
Peridotitic data - Literature

Figure 8

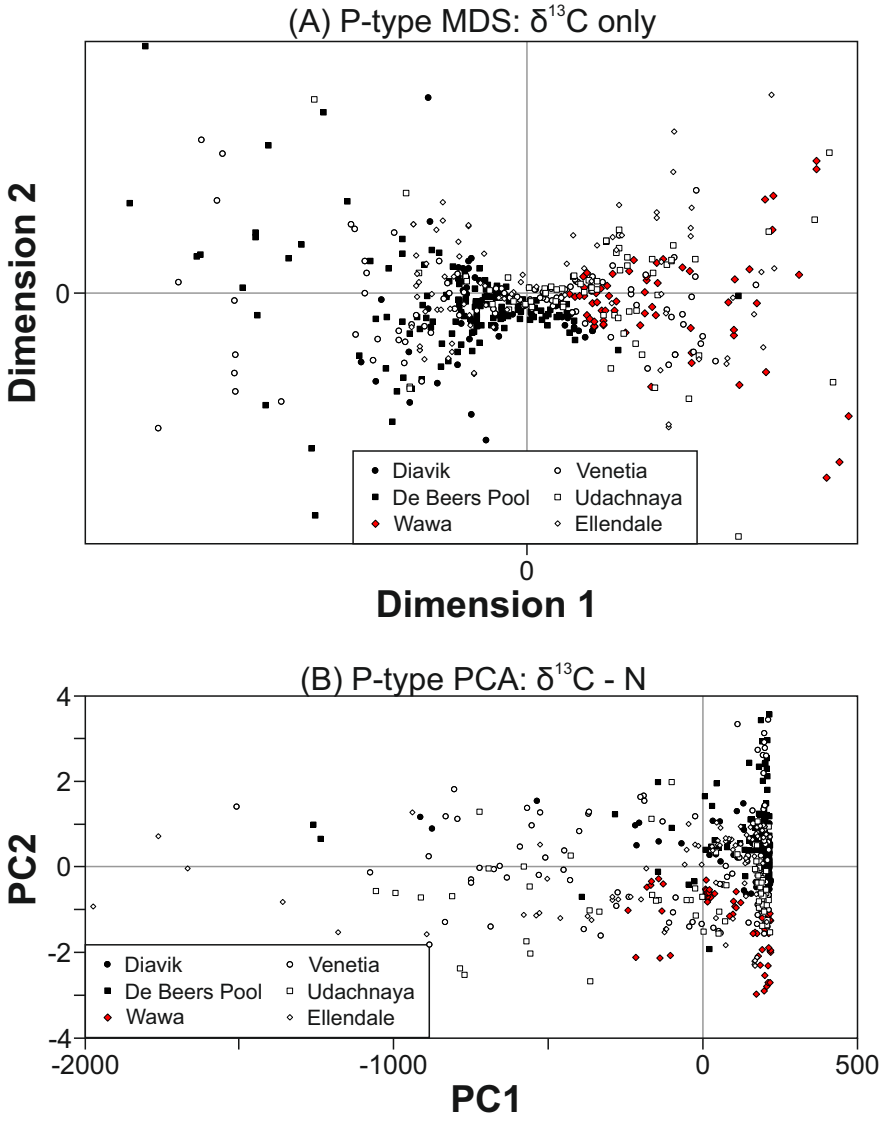
(A) P-type MDS: δ13C only
Dimension 2
0
0
Dimension 1
Diavik
De Beers Pool
Wawa
Venetia
Udachnaya
Ellendale
(B) P-type PCA: δ13C - N
PC2
4
2
0
-2
-4
-2000
-1000
0
500
PC1
Diavik
De Beers Pool
Wawa
Venetia
Udachnaya
Ellendale

Figure 9

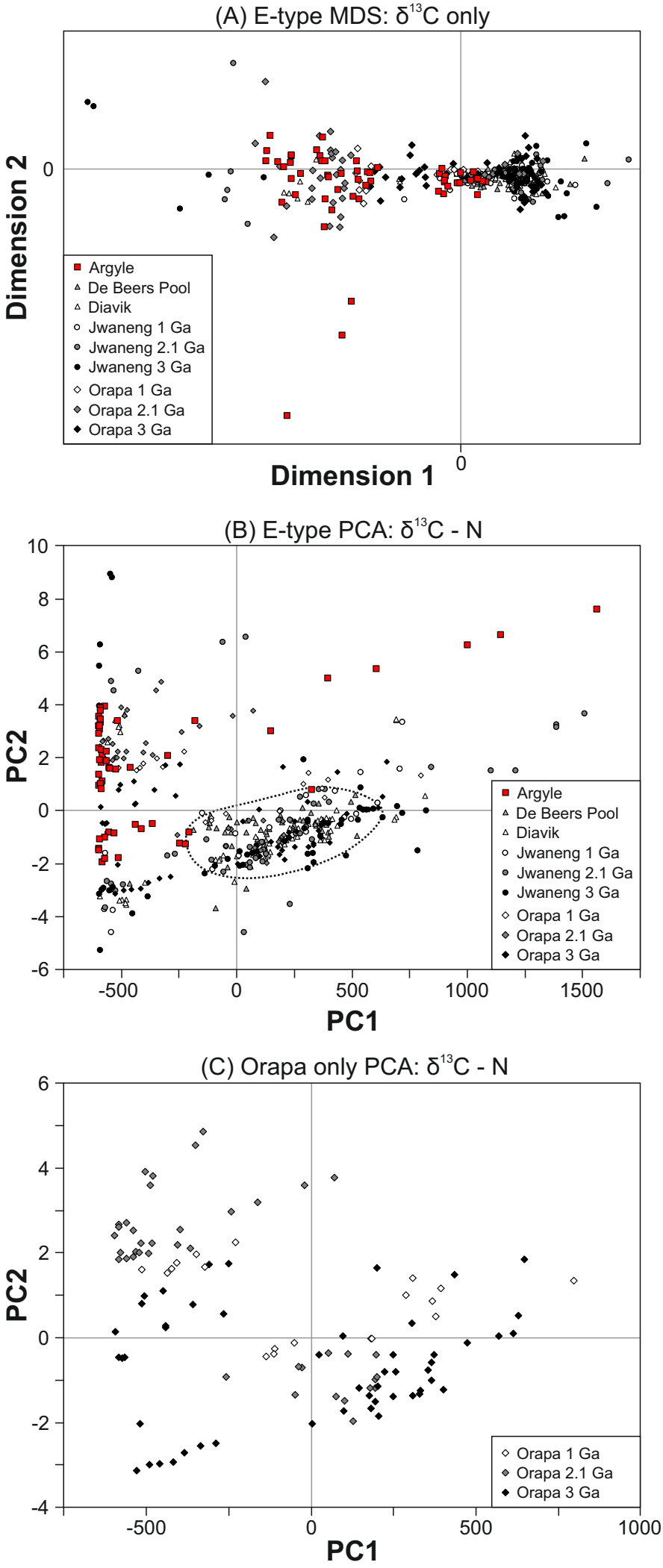
(A) E-type MDS: δ13C only
Dimension 2
Dimension 1
0
0
Argyle
De Beers Pool
Diavik
Jwaneng 1 Ga
Jwaneng 2.1 Ga
Jwaneng 3 Ga
Orapa 1 Ga
Orapa 2.1 Ga
Orapa 3 Ga
(B) E-type PCA: δ13C - N
PC2
PC1
10
8
6
4
2
0
-2
-4
-6
-500
0
500
1000
1500
Argyle
De Beers Pool
Diavik
Jwaneng 1 Ga
Jwaneng 2.1 Ga
Jwaneng 3 Ga
Orapa 1 Ga
Orapa 2.1 Ga
Orapa 3 Ga
(C) Orapa only PCA: δ13C - N
PC2
PC1
6
4
2
0
-2
-4
-500
0
500
1000
Orapa 1 Ga
Orapa 2.1 Ga
Orapa 3 Ga